Journal of Visualized Experiments

Quantifying the brain metastatic tumor micro-environment using an organ-on-a chip 3D model, machine learning, and confocal tomography.

--Manuscript Draft--

Article Type:	Invited Methods Article - JoVE Produced Video
Manuscript Number:	JoVE61654R1
Full Title:	Quantifying the brain metastatic tumor micro-environment using an organ-on-a chip 3D model, machine learning, and confocal tomography.
Section/Category:	JoVE Cancer Research
Keywords:	metastasis, tumor; microenvironment; cancer; organ-on-a-chip; Machine learning; Artificial intelligence; confocal microscopy; long-term cell culture, model
Corresponding Author:	Christopher Ryan Oliver, Ph.D. University of Michigan Ann Arbor, Michigan UNITED STATES
Corresponding Author's Institution:	University of Michigan
Corresponding Author E-Mail:	croliver@umich.edu
Order of Authors:	C. Ryan Oliver, Ph.D.
	Trisha M. Westerhof
	Maria G. Castro
	Sofia D. Merajver
Additional Information:	
Question	**Response**
Please indicate whether this article will be Standard Access or Open Access.	Standard Access (US$2,400)
Please indicate the **city, state/province, and country** where this article will be **filmed**. Please do not use abbreviations.	Ann Arbor, MI, USA

ROGEL CANCER CENTER
MICHIGAN MEDICINE

Sofia D. Merajver, MD Ph.D.
Professor of Internal Medicine
Sofia Merajver Laboratory
7111 Cancer Center
1500 E Medical Center Dr
Ann Arbor, Michigan 48109
734 763-6009 lab
smerajve@med.umich.edu

July 1, 2020

Dear Dr. Jaydev Upponi,

Thank you for the invitation to submit our manuscript titled "Quantifying the brain metastatic tumor micro-environment using an organ-on-a chip 3D model, machine learning, and confocal tomography." for consideration to be published in *JoVE* as part of the *Preclinical models and imaging modalities of tumor microenvironment in metastasis* Methods Collection.

We appreciate the reviewers and editors' thorough review to ensure our manuscript meets the exacting standards of JoVE. Please find the revised manuscript enclosed which we believe has significantly improved the manuscript and addressed the reviewer's comments. We look forward to your response and are able to provide any additional information you may require.

Once again, I want to re-iterate that we believe this work will be of great interest to and be cited by the readership of *JoVE* due to its comprehensive approach to imaging and analyzing the tumor microenvironment during metastasis in a preclinical model. Thank you for considering our manuscript and we look forward to hearing from you.

Cordially yours,

Sofia D. Merajver, MD PhD
Professor of Internal Medicine and Epidemiology
Scientific Director, Breast Oncology Program
Director, Breast and Ovarian Cancer Risk Evaluation Program
Rogel Cancer Center
University of Michigan
Ann Arbor, Michigan, USA

JOURNAL OF VISUALIZED EXPERIMENTS
1 Alewife Center #200
Cambridge, MA 02140
tel. 617.945.9051
www.jove.com

TITLE:

Quantifying the Brain Metastatic Tumor Micro-Environment using an Organ-On-A Chip 3D Model, Machine Learning, and Confocal Tomography

AUTHORS AND AFFILIATION:

C. Ryan Oliver[1,2,*], Trisha M. Westerhof[1,2,*], Maria G. Castro[2,3,4], Sofia D. Merajver[1,2]

[1]Department of Internal Medicine, University of Michigan Ann Arbor
[2]Rogel Cancer Center, University of Michigan Ann Arbor
[3]Department of Neurosurgery, University of Michigan Ann Arbor
[4]Department of Cell and Developmental Biology, University of Michigan Ann Arbor
*These authors contributed equally.

Email addresses of co-authors:
C. Ryan Oliver (croliver@umich.edu)
Trisha M. Westerhof (tmwester@med.umich.edu)
Maria G. Castro (mariacas@med.umich.edu)

Corresponding author:
Sofia D. Merajver (smerajve@umich.edu)

KEYWORDS:

Tumor, microenvironment, cancer, organ-on-a-chip, machine learning, artificial intelligence, confocal microscopy, long-term cell culture.

SUMMARY:

Here, we present a protocol for preparing and culturing a blood brain barrier metastatic tumor micro-environment and then quantifying its state using confocal imaging and artificial intelligence (machine learning).

ABSTRACT:

Brain metastases are the most lethal cancer lesions; 10-30% of all cancers metastasize to the brain, with a median survival of only ~5-20 months, depending on the cancer type. To reduce the brain metastatic tumor burden, gaps in basic and translational knowledge need to be addressed. Major challenges include a paucity of reproducible preclinical models and associated tools. Three-dimensional models of brain metastasis can yield the relevant molecular and phenotypic data used to address these needs when combined with dedicated analysis tools. Moreover, compared to murine models, organ-on-a-chip models of patient tumor cells traversing the blood brain barrier into the brain microenvironment generate results rapidly and are more interpretable with quantitative methods, thus amenable to high throughput testing. Here we describe and demonstrate the use of a novel 3D microfluidic blood brain niche (µmBBN) platform where multiple elements of the niche can be cultured for an extended period (several days), fluorescently imaged by confocal microscopy, and the images reconstructed using an innovative confocal tomography technique; all aimed to understand the development of micro-metastasis

and changes to the tumor micro-environment (TME) in a repeatable and quantitative manner. We demonstrate how to fabricate, seed, image, and analyze the cancer cells and TME cellular and humoral components, using this platform. Moreover, we show how artificial intelligence (AI) is used to identify the intrinsic phenotypic differences of cancer cells that are capable of transit through a model μmBBN and to assign them an objective index of brain metastatic potential. The data sets generated by this method can be used to answer basic and translational questions about metastasis, the efficacy of therapeutic strategies, and the role of the TME in both.

INTRODUCTION:

Brain metastases are the most lethal cancer lesions; 10-30% of all cancers metastasize to the brain, with a median survival of only ~5-20 months, depending on the cancer type[1,2]. A principal question that arises when studying cancer metastasis is how sub clones migrate from the humoral environment of the bloodstream into an organ such as the brain[3,4]. This question has led to many variations of migration, invasion, and extravasation assays. All these methods share the critical step of counting or measuring properties of cells that move from one location to another in response to a stimulus. Most migration assays readily available are used to study two-dimensional (2D) migration of cancer cells. These have elucidated a wealth of knowledge; however, they do not recapitulate the three-dimensional nature of the in vivo system that other methods can provide[5]. Therefore, it is necessary to study the tumor micro-environment (TME) in three-dimensional (3D) systems, but the analysis approaches available for 3D structures are limited and often inconsistent.

One of the most popular 3D tools is a Boyden chamber that consists of a membrane suspended at the bottom of a well, separating two distinct regions. Boyden introduced the assay to study leukocyte chemotaxis[4]. The bottom regions may be varied by chemistry or other means[6,7] to induce cells in the upper region to migrate to the lower region. The most common approach to quantifying the number of cells that have migrated is to release the cells from the bottom of the membrane using a buffer solution, lyse them, and then count them based on the quantity of DNA content in the solution[7]. This indirect approach is prone to operator error due to technique variability and the procedure destroys information about the cancer phenotype and the micro-environment. Variations of the Boyden chamber assay involve fixation of migratory cells that remain on the membrane, but only provides a count of cells that are no longer viable for continued study[6,8,9].

Due to limitations of the Boyden chamber and the growth of innovations in the microfluidic community, migration assay chips have been developed which observe the motion of cells in response to a stimulus in one direction rather than three[10-12]. These migration assays facilitate control over factors such as flow or single cell separation[13,14] that enable better interpretation of the results; however, their 2D format inevitably loses some dynamic information. Recent studies have focused on extravasation (i.e., the movement of cells from circulation into a tissue, such as the blood brain barrier) in a 3D environment[14,15]. The extravasation distance into tissue and probing behavior that occurs at the cellular barrier/membrane is more refined than measurements gleaned using either the Boyden chamber or a 2D microfluidic migration device[16]. Thus, devices that enable appropriate imaging and analysis of 3D extravasation are critical to

capture these sophisticated measurements but are lacking in the literature.

Independent of migration assays, robust imaging techniques have been developed for magnetic resonance imaging (MRI) and tomography that are able to identify and accurately reconstruct tissue in 3D space[17,18]. These techniques acquire images in z-stacks and segment portions of the image based on the properties of the tissue and then convert the segmented images into three-dimensional meshes[19-21]. This allows physicians to visualize in 3D individual organs, bones, and vessels to aid in surgical planning or aid in diagnosis of cancer or heart disease[22,23]. Here, we will show that these approaches can be adapted for use on microscopic specimens and 3D extravasation devices.

To this end, we developed the innovative confocal tomography technique, presented herein, which affords flexibility to study the extravasation of tumor cells across a membrane by adapting existing tomography tools. This approach enables the study of the full gamut of cancer cell behaviors as they interact with a cellular barrier, such as an endothelial cell layer. Cancer cells exhibit probing behaviors; some may invade but remain close to the membrane, while others traverse the barrier readily. This technique is capable of yielding information about the phenotype of the cell in all dimensions[24]. Using this approach to study the TME is both relatively inexpensive, easy to interpret, and reproducible, when compared to more complex in vivo murine models. The presented methodology should provide a strong basis for the study of many types of tumors and micro-environments by adapting the stromal region.

We describe and demonstrate the use of a 3D microfluidic blood brain niche (µmBBN) platform (**Figure 1**) where critical elements of the barrier and niche (brain microvascular endothelial cells and astrocytes) can be cultured for an extended period (approximately up to 9 days), fluorescently imaged by confocal microscopy, and the images reconstructed using our confocal tomography technique (**Figure 2**); all aimed to understand the development of micro-metastasis and changes to the tumor micro-environment in a repeatable and quantitative manner. The blood brain barrier interface with the brain niche is composed of brain microvascular endothelial cells that are strengthened by basement membrane, astrocyte feet, and pericytes[25]. We selectively focused on the astrocyte and endothelial components given their importance in the formation and regulation of the blood brain barrier. We demonstrate how to fabricate, seed, image, and analyze the cancer cells and tumor micro-environment cellular and humoral components, using this platform. Finally, we show how machine learning can be used to identify the intrinsic phenotypic differences of cancer cells that are capable of transit through a model µmBBN and to assign them an objective index of brain metastatic potential[24]. The data sets generated by this method can be used to answer basic and translational questions about metastasis, therapeutic strategies, and the role of the TME in both.

PROTOCOL:

1. **Prepare the blood brain barrier niche mold**

NOTE: The culturing device used in this platform is a PDMS based scaffold that we build a cellular

blood brain barrier niche upon. It is made of two parts separated by a porous membrane. To prepare the blood brain barrier niche two SU-8 molds made using photolithography are necessary[26,27]. The protocol will be described for the 100 µm thick mold first and then notes will be given for the 200 µm thick mold.

1.1 To prepare the mold, clean a 4" silicon wafer using acetone with a squeeze bottle and then dry it with a nitrogen gun.

1.1.1 Bake the silicon wafer on a hotplate for 10 min at 200 °C to remove all residual solvent.

1.1.2 In turn center the silicon wafer onto the chuck of a spin coater and dispense 1 mL of SU8-2075 for the top mold. Spin for 5 s at 500 rpm (acceleration 300 rpm/s) to disperse the photoresist and then 30 s at 2200 rpm (acceleration 300 rpm/s) to obtain a 100 µm thick SU-8 coating. Optimization may be necessary to achieve the specified thickness.

1.2 Soft bake the wafer on a hotplate at 65 °C for 2 min and then immediately at 98 °C for 20 min.

1.3 Place the wafer into a photolithography lamp and position the mask centered onto the wafer according to standard procedures. Expose the SU-8 coated wafers with a radiance of 230 mJ/cm^2 of UVB (360 nm ± 10 nm). An exposure matrix experiment may be performed to determine the optimum dosage. Mask designs are available in **Supplemental File 1**.

1.4 Perform a post-exposure bake at 65 °C for 2 min and then immediately at 98 °C for 10 min to improve adhesion. Cool the wafer to 50 °C.

1.5 Remove the un-exposed resist using SU-8 photo-developer. Rinse the wafer in developer for 5 min in a bath and then use a spray bottle filled with SU-8 developer in a chemical hood to agitate and remove remaining uncured SU-8. A 4x microscope can be used to observe if all the uncured SU-8 has been removed. A white line on the edges of the photoresist features indicates the SU-8 has not been removed fully.

1.6 Perform a final hard bake in an oven at 110 °C for 60 min.

1.7 Follow the same procedure for the 200 µm thick mold using SU-8 2075 but adjust the protocol to the following:

1.7.1 Spin coater settings: Spin for 5 s at 500 rpm (acceleration 300 rpm/s) to disperse the photoresist and then 30 s at 1300 RPM (acceleration 300 rpm/s) to obtain a 200 µm thick coating.

1.7.2 Soft bake at 65 °C for 2 min then at 98 °C for 40 min.

1.7.3 Exposure time of 340 mJ/cm^2.

1.7.4 Post exposure bake: 2 min at 65 °C, and then 98 °C for 15 min.

1.8 Finally, silanize each wafer by placing them in a vacuum chamber inside of a chemical hood with a plastic container in which 3 drops (~150 µL) of silanizing solution (Trichloro perfluoro octyl silane) have been placed. Pull a vacuum and leave overnight to allow the vapor to coat the wafer. This step reduces adhesion between the SU-8 and PDMS, increasing the life of the mold.

CAUTION: Trichloro perfluoroctyl silane should be always handled in the fume hood and kept away from water sources.

1.9 Place individual wafer molds into 150 mm Petri dishes using two strips of double-sided tape. Ensure the wafers are flat. An alternative is to fabricate an aluminum mold within which the wafer can be placed. Because the aluminum mold is enclosed it will produce casts with a uniform thickness, whereas the Petri dish method is sensitive to the tilt of the surface is it placed on. The improved flatness of the PDMS casts reduces downstream confocal imaging time.

2. Form and assemble the PDMS blood brain barrier (BBB) device

2.1 Mix 75 g of PDMS at a ratio of 1:10 (Crosslinker:Base) by weight in a plastic cup.

2.2 Pour the PDMS over the molds (1 mm thick for the 200 µm thick mold and 4 mm for the 100 µm thick mold) and degas in a vacuum desiccator for one hour or until all the bubbles have been removed. Place in a 65 °C oven overnight. The 1 mm thickness may be adjusted based on the working distance of the 10x objective in the confocal microscope.

2.3 After the PDMS has cured use a blade to gently cut against the wafer through the PDMS around the edges. Peel the PDMS off and use a blade to cut along the rectangular guides and a 1.5 mm biopsy punch to open the inlets and outlets on the device. Cover the PDMS device parts with 48 mm wide packing tape to keep it clean from dust and debris.

2.4 Next use dissection scissors to cut a 5 mm x 50 mm rectangle of polycarbonate membrane with 5 µm pores and store it inside of a Petri dish for later use.

2.5 Gather the following: 200 µL pipette tip, 2 mL of 1:10 PDMS mixed with toluene at a ratio of 2:3 by weight in a glass vial, a Pasteur pipette with a squeeze bulb, the prepared PDMS upper and lower parts, the membrane, three 50 mm x 75 mm glass slides and transport it all to a spin coater. The following steps for assembly and cell seeding of the device are depicted in **Figure 1**.

2.6 Use the Pasteur pipette to transfer 1 mL of PDMS:toluene glue solution into a 50 mm x 75 mm glass slide on the chuck of the spin coater. Spin for 5 seconds at 100 rpm (acceleration 300 rpm/s) and 30 seconds at 2000 rpm (acceleration 300 rpm/s).

2.7 Place the slide on a table and cover it with one PDMS upper chamber and one lower chamber so that the PDMS faces with features molded into it contact the slide and the glue is

transferred to the PDMS face, outlining the perimeter of all features.

2.8 Flip the PDMS upper chamber onto another slide with the glue coating facing up and carefully place the membrane across the device between the inlets and outlets. Place the 200 µL tip in the PDMS:toluene glue solution until it has wicked some into the tip. Touch the tip between each inlet and outlet to place a small drop near the edge of the membrane where it contacts the PDMS.

2.9 Remove the other half of the device and place it on with the glue coating down while aligning the inlets and outlets on the two parts.

2.10 Place the assembled device into an oven at 37 °C overnight to cure the glue. Transfer to a vacuum bell jar with desiccant and let dehydrate for two days. This is a crucial step to allow the Toluene to evaporate and to improve the consistency of seeding the device by regulating the absorbed water vapor in the laboratory air.

3. Seed the brain micro-environment into the device

3.1 Cell culture and reagents: Before beginning this protocol, obtain the following reagents and cells. Cultivate all cell lines in an incubator set at 37 °C in 5% CO_2.

3.1.1 Maintain human triple-negative breast cancer cell line MDA-MB-231 (ATCC HTB-26) and MDA-MB-231-BR-GFP cells (obtained from Patricia Steeg, PhD) in DMEM with 4.5 g/L glucose, supplemented with 2 mM L-glutamine, 10% FBS and 1x antibiotic-antimycotic. Create MDA-MB-231-GFP fluorescent cells by transducing MDA-MB-231 cell with empty vector pLL-EV-GFP lentivirus. Sort the transduced GFP^+ population using fluorescence-activated cell sorting (FACS) prior to experimentation.

3.1.2 Maintain human brain microvascular endothelial cells hCMEC/D3 in EGM-2 medium. Create hCMEC/D3-DsRed fluorescent cells by transducing hCMEC/D3 with empty vector pLL-3.7-dsRed lentivirus. Remove all non-transduced, non-fluorescent cells from the culture using FACS prior to experimental use.

3.1.3 Maintain normal human astrocytes (NHA) in DMEM supplemented with 4.5 g/L glucose, 10% FBS, 2 mM Glutamax, 1 mM sodium pyruvate, 1x N-2 growth supplement, and 1x antibiotic-antimycotic. Immortalize the astrocytes by transducing pLOX-TERT-iresTK lentiviral vector (Addgene 12245). Create the vector using plasmid psPAX2 and envelope plasmid pMD2.G (Addgene 12260 and 12259).

3.2 Remove a µmBBN device from the vacuum desiccator and place onto a metal or paper (i.e., tape) surface with the inlets facing down and put it into a plasma chamber. Also place a 50 mm x 75 mm glass slide into the plasma chamber. Pull a vacuum and then treat with plasma at 80 W for 30 s.

3.3 Quickly remove the glass slide and device from the plasma chamber and place the device with the inlets facing up onto the glass slide aligned using a guide (**Supplemental File 2**). This will create a permanent bond between the PDMS and glass slide and cannot be re-positioned.

3.4 Next cut the tips off 16, 200 µL pipette tips, 2 mm from the tip. Insert the pipette tips into all the inlets and outlets. The device can be placed back into the vacuum desiccator at this point if not ready to seed the cells.

3.5 Place the device back in the plasma chamber and treat with plasma for 8 min at 200 W. After the device has cooled (5 min) from the plasma treatment place it inside a sterile secondary container, like a transparent pipette tip box. Perform the next step within ~15 min or the effectiveness of the plasma treatment may be reduced leading to clogging.

3.6 Several days before the experiment culture Petri dishes of 1 x 10^6 endothelial cells (hCMEC/D3-DsRed) and 1 x 10^6 astrocytes (NHA). While the device is undergoing the 8 min plasma treatment, prepare a collagen solution consisting of 0.5 mL of 3 mg/mL PureCol type I bovine collagen with 64 µL of 0.8 M $NaHCO_3$ and 20 µL of 10x high-glucose (250 mM) MEM. Suspend 5.0 x 10^5 NHA cells in the collagen solution. Maintain the solution on ice while not in use.

3.7 Transfer 120 µL of the collagen/astrocyte/microglia solution into the device through the pipette tip for the bottom chamber (**Figure 1 Red arrows**). Allow the solution to wick across the chamber into the opposite pipette tip. After all four channels of the device have been filled place the chip in the CO_2 incubator at 37 °C and 5% CO_2 for 1 h or until the collagen has set.

3.8 After the collagen sets, fill all pipette tips feeding the bottom chamber with a mixture of complete media. For chips containing endothelial cells and astrocytes, a 50:50 mix of endothelial:astrocyte media is used.

3.9 Coat the upper chamber with 2% growth-factor reduced Matrigel in complete endothelial media using the upper chamber pipette tip (**Figure 1 Blue arrows**) and place in the incubator for 1 hr.

3.10 Rinse the upper chamber with the indicated media mixture and alternate which tip is seeded with endothelial cells (**Figure 1 Green arrows**). Suspend 1 x 10^6 endothelial cells in 1 mL of endothelial media and seed 30 µL every 15 min into alternating upper chamber tips for even coverage. Seed endothelial cells into each upper chamber tip twice, for a total of 4 times per chamber.

3.11 After the final seeding of endothelial cells, fill all the tips with the media mixture and place the device in the incubator at 37 °C and 5% CO_2, changing media in both chambers every 12 h.

4. Monitor progression of the endothelial layer formation

4.1 Complete coverage of the channel by the endothelial layer is observed after 3 days. Use one of two methods to monitor the coverage of the endothelial barrier: Fluorescence or TEER. the hCMEC/D3-DsRed fluorescence and according % coverage across the channel area can be quantified using ImageJ.

4.1.1 Open the TIFF file in ImageJ representative of the hCMEC/D3-DsRed barrier. In the ImageJ software, click **File > Open** to select the file.

4.1.2 Merge all the Z-layers of the image using the maximum intensity following these key commands and options: **Image > Stacks > Z project > All Z slices, Maximum intensity**.

4.1.3 Perform a color threshold that is the same across all microfluidic chips assessed using this method. For the study presented we employed a threshold of 450. Use the threshold menu in ImageJ at: **Image > Adjust > Threshold**.

4.1.4 Set the measurements to be recorded using the following commands and options: **Analyze > Set Measurements > Limit to threshold, Area Fraction**.

4.1.5 Select a representative region of the microfluidic channel to measure by drawing a box. The box tool is located on the main menu of ImageJ. Measure 3 technical replicates positioned at the beginning, middle, and end of each microfluidic channel using the same box size.

4.1.6 Analyze each channel and record the area fraction, representing the % endothelial coverage. Export these measurements as spreadsheet files to plot and visualize the data using the following commands: **Analyze > Measure**.

4.2 As an alternative, use Impedance spectroscopy-based TEER to measure endothelial tight junctions per area. Quantification of the endothelial barrier using TEER is a proxy for the integrity of the endothelial layer as a barrier.

4.2.1 Position two electrodes in the inlet and outlet of the upper and lower chambers.

4.2.2 Quantify the impedance of the endothelial monolayer as a combination of the resistances, inductances, and capacitances in the chip according to a model proposed by Srinivasan et al.[28,29].

5. Seed cancer cells into the device

5.1 After the endothelial layer has matured, seed cancer cells into the device. Prepare a 1 mL solution of 1 x 10^6 cancer cells in complete cancer cell media.

5.2 Exchange the media in the chip to replenish cell culture nutrients.

5.3 Seed each top chamber channel with 30 µL of cancer cells in suspension and then place

the device back in the incubator for a 15 min. Always seed the cancer cells on the same side of all four top chamber channels within a single device.

5.4 Exchange the device with new media and the refill the tips every 12 hours until the device is imaged for metastatic behavior.

6. Image the tumor micro-environment by confocal imaging

6.1 At the desired experimental timepoint (1, 2, or 9-days), use confocal imaging to capture a 3D image of the channel. We perform this step on a Nikon A1 using the settings described here. This step is automated, and each channel requires 20-40 min to image depending on how many fluorescent channels are included and the Z-depth needed to cover the positions of all the cells.

6.2 Turn the microscope on, open the software and place the incubator cover onto the microscope.

6.3 Set the microscope stage heater to 37 °C and CO_2 to 5% if available.

6.4 After the microscope incubator has stabilized, place the device into the microscope stage using the 50 mm x 75 mm mount.

6.5 Focus on one side of the device (left if to be used with the provided analysis software) with a 10x objective and set the Z height as zero. Under z-stack settings, include a range of 100 µm above and 200 µm below the focus plane. Then use the stitching setting to set the number of X and Y fields to 1 and 9 respectively with 15% overlap. Set the pinhole to its recommended minimum and the z-layer height to 9 µm. Adjust the bright field exposure so that the porous membrane is visible. Turn on the excitation lasers for the dsRed (561 nm) and GFP (488 nm) channels and adjust the fluorescent laser powers and cutoffs so that each channel is visible without overexposing the pixels.

6.6 Verify all fields are in focus when stepped over. If so, enter an output file name (001.nd2) for the image and start the experiment to automatically capture the 3D confocal image.

7. Measure the tumor micro-environment via confocal tomography

7.1 Use confocal tomography an approach to estimate a set of metrics and measurements that describe the individual cells and the tumor micro-environment within the device. Confocal tomographic analysis (**Figure 2**) converts a confocal z-stack into a three-dimensional representation of the cells. Using a custom python script within the Jupyter notebook/lab environment, a plane is then matched to the layer of cells which form the blood brain barrier like membrane [30]. Finally, make phenotypic measurements of the cancer cell populations (**Table 1**).

7.1.1. Perform this analysis at the end of an experiment or over a time course. Install python and the appropriate libraries according to the referenced software guide, then open the software

from Windows Command Prompt by running the command “conda activate”, followed by “jupyter lab”. The Jupyter environment will load within the default browser.

7.1.2. From the Jupyter file explorer double click the Jupyter notebook “contom.ipynb” to open it. Run the cell below the title **Import libraries, custom classes/functions and setup the notebook** by clicking the notebook cell and then clicking the play button. All notebook cells below are executed using the same approach. Note that here notebook “cell” refers to a block of python code within the Jupyter notebook.

7.2 Prepare the data. This algorithm uses the visualization toolkit (VTK) to manipulate and display the z-stack and three-dimensional data[17].

7.2.1. Place the provided .XLSX file (“Experiment Tracker.xlsx”) in the same windows folder as the Jupyter notebook. The file tracks experiments and interfaces with the Jupyter notebook. Place the ND2 file from section 6 into a subfolder called “\Experiment_XXX\Confocal\” below the Jupyter notebook location. Additional experiment folders can be added within by adjusting the “XXX” to the numerical ID assigned to new folders.

7.2.2. Label the first experiment folder “Experiment_001” and the ND2 file “001.nd2”. First, convert the ND2 imaging file into a stitched multi-image TIFF file separated by color channel. Do this by executing the notebook cell below the title “Read the confocal z stack into memory” with the Save_tiff_from_ND2 () function uncommented[30]. The ND2 file is a proprietary imaging format from Nikon, thus it is necessary to convert it to a format that open source software is compatible with.

NOTE: The TIFF (Tag Image File Format) is used because it is ubiquitous, 16 bit compatible, easily imported into VTK, and multiple images can be stored in a single file, which is appropriate for z-stack images. Executing the notebook cell will read in an image from the ND2 file, extract information of the color and XYZ positions then store that image in a numpy array according to a pre-determined structure. It will then save the array as a TIFF file using the python library tifffile.

7.3 Convert imaging data into 3D model

7.3.1. Import the TIFF file into VTK (vtkTIFFReader) using a 3D rendering to visualize the cells (**Figure 2**). Select a threshold based on the color of the cells in the image. To clarify, the VTK object represents a block of pixels (X, Y, Z) in space (volume) but only certain pixels (green or red) represents cells, the rest are background or noise (black).

7.3.2. Therefore, set an opacity filter on the volume which removes the background confirm that what fluorescence remains is only the cells. Do this using the Jupyter notebook cell titled, **Change opacity values for each microscope channel** by adjusting the Channel_alpha value variables (i.e., GFP_alpha). Visualize the effect using the notebook cell titled **View a 3D rendering to verify the threshold are set correctly**.

7.3.3. Save the opacity values in the spreadsheet to use in the next step. Convert the volume data into individual 3D objects, each representing a cell in the image using a technique called marching cubes[31]. This algorithm extracts a polygonal mesh of an isosurface from three-dimensional discrete scalar fields of voxels.

7.3.4. Use the opacity value in the marching cubes algorithm to separate each cell from the background. Complete this step for all fluorescent cells identified in each microscope channel by running **Convert voxel image into a triangular mesh and save as a VTK file** in the notebook.

7.4 Fitting a plane to the membrane

7.4.1. Fit a plane to the endothelial barrier by first locating the cell centroids (notebook cell: **Analyze the RFP channel** (**endothelial barrier**)). Iterate through the list meshes in the volume and extract the regions that are not connected using a PolyDataConnectivityFilter from VTK. Calculate the centroid of each mesh and add the measurement to a list of centroids filtering for meshes that are too large or too small (<50, >1000000 voxels).

7.4.2. Fit a plane to the list of centroids for the endothelial cells using a minimization of error method (notebook cell: **Fit a plane to the RFP centroids (endothelial barrier)**) (**Figure 2, Figure 3**)[32]. Inspect the fit of the plane by plotting the plane and centroids and adjust manually if necessary (using theta, beta and z) by running the notebook cell titled **Visualize RFP centroids and plane fit**.

7.4.3. After the plane is properly fitted, save the normal of the plane to the Experiment Tracker File .XLSX file for future use.

7.5 Analyze the descriptive features of individual cancer cells for the following descriptors (**Table 1**).

NOTE: If the computer performing the analysis is lagging, high throughput analysis via high performance computing is an option. This algorithm is useful on standard laptops for the analysis of small numbers of cells, however VTK is not well suited to a large number of individual objects (>1000). Therefore, it is optional to use the adapted algorithm to function on a high-performance computing cluster. This enables rapid analysis of experiments with many cells (**Figure 2**). All of 7.5 is accomplished by running the notebook cells titled **Analyze the remaining microscope channels for phenotypic descriptors** and **Read in the Experiment_tracker information and analyze the channels that exist**.

7.5.1 Measure the extravasation of the cancer cells: After characterizing the endothelial layer with a plane, measure the volume of each cancer cell that has migrated through the membrane. Clip each cell (Boolean) so that the mesh below the membrane is kept and the portion above the membrane is removed[33]. Then close the open mesh (vtkFillHoles).

7.5.1.1. Recalculate the normal and the new centroid of the clipped mesh. Measure the

volume and position of each clipped cancer cell for analysis. Volume is equivalent to the number of voxels the mesh fills of each single cell. Calculate the distance between the endothelial plane and position of each cancer cell.

7.5.2 Measure the cellular phenotype: Calculate the morphology of each cancer cell by factoring its shape, volume and position.

7.6 Validate the measurements and save to a spreadsheet or plot. Run the notebook cell titled **Check that centroids were measured accurately** and a render will pop up showing the centroids identified on top of the imaged volume by cell type. After all the experiments are done export the complete data set as a single spreadsheet file by typing the experiments to be included by ID in the notebook cell titled Exp**ort the data as a single Data.XLSX file** for the variables **experiments** replacing the given experiment IDs. If verify the completed data set, plot it using the notebook cell titled **Distance extravasated strip plot**. The plot will appear in the notebook environment and save to file.

8. **Analyze the related characteristics using Artificial Intelligence**

NOTE: Identify metastatic phenotypic features using artificial intelligence algorithms.

8.1 Perform binary classification using Orange according to the scheme shown in **Figure 5** and **Supplemental File 3**. Start Orange from a second Windows Command Prompt by typing "conda activate" followed by "python -m Orange.canvas" and click **New** from the prompt. Orange is drag and drop based software, so arrange the functions by dragging each item from the left menu onto the canvas to match **Supplemental File 3**. After that is complete double click the **File** icon and select the Data.XLSX file.

8.2 Filter the data to remove bad measurements, defined as those that failed a Boolean operation or giving parametric variable values outside of known bounds using the "Select Rows" icon. Double click the icon and set conditions that correspond to the filter such as "Sphericity is between 0 and 1". Create conditions for 8.2.1, 8.2.2 and 8.2.3.

8.2.1 Filter distance extravasated measurements to range from -100-200 µm.

8.2.2 Filter sphericity measurements of cell shape to range from 0-1.

8.2.3 Filter cancer cell volume measurements to range from 0-2000 voxels.

8.2.4 Use all parametric variables (**Table 1**) to classify brain-metastatic MDA-MB-231-BR-GFP and non-brain metastatic MDA-MB-231-GFP. Double click **Select Columns** icon from the canvas. Using the **>** button to move **Available Variables** into either **Features**, **Target Variables**, or **Meta Attributes**. The only variable that should be a **Target Variable** is a Metastatic label which defines if cells in the data set are considered metastatic (1) or not (0). Experiment variables can be placed in the **Meta Attributes** section.

8.3 Sample the data into a training (80%) and test set (20%). Double click the **Data sampler** icon and select a Sampling type of **Fixed proportion of data:** set to 80% and select replicable and stratify check boxes. Stratify and cross-validate the training set using 10 folds against each model/classifier. Double click **Test & Score** and select **Cross validation** with **Number of folds:** set to 10 and **Stratified** checked. Set the **target class** to **1**.

8.4 In this method, use Neural Networks and Random Forest learning algorithms as they are robust to the data. Within the **Random Forest** icon, choose the **Number of Trees** to be 50 and did not select any other options. Within the **Neural Network** icon choose **Neurons per hidden laye**r: **100**, **Activation: ReLu**, **Solver: Adam**, **Alpha: 0.0001**, and **Max Iterations: 200**. However, these settings will vary significantly by study and should be well understood before application.

8.5 After setting up the canvas double click each icon from **File** to **Sample Data** and either hit **Apply** or **Send Data**. Double click **Test & Score** and the training data will begin to be used to develop a model using the algorithms. After training the machine learning model, re-open **Test & Score** and select **Test on Test Data** and close the popup window to score the performance of the model by classifying the cells in the chip according to the probability they are brain metastatic from 0 to 1.

8.6 Save the machine learning model performance to a file (**Table 2**). Include the area under the curve (AUC) of the ROC, the accuracy and the F1 score. Save a second file that contains the individual metastatic indices and classification probabilities. Double click the **Save** icon and click **Save As** to write to file the classification probabilities. Similarly, the ROC curve can be viewed by double clicking **ROC Analysis** icon and the model performance can be calculated by double clicking the **Confusion Matrix** icon.

REPRESENTATIVE RESULTS:

Using this technique, we analyzed cell types labeled with different fluorescent proteins or dyes. We demonstrate the use of this approach with a µmBBN chip formulated with hCMEC/D3-DsRed and non-fluorescent astrocytes. The brain microvascular endothelial cells were seeded onto a porous membrane (5 µm track etched pores) and placed in an incubator[34] at 37 °C under 5% CO_2. After three days the confluency of the endothelial layer was confirmed via microscopy and then cancer cells were placed on top of the endothelial layer. Two breast cancer cell lines, a brain-seeking clone termed MDA-MB-231-BR-GFP, and parental MDA-MB-231-GFP cells were input into the µmBBN chip containing an astrocytic brain niche[35-41]. The µmBBN chips were imaged at 1, 2, and 9-Days using a confocal microscope with 3 channels (dsRed, GFP and Brightfield) using a 10x objective, with Z-slices every 9 µm and 1x9 XY stitching to cover the entire membrane area. This microscope maintained a temperature of 37 °C during the imaging process to minimize stress on the cells.

A representative image of a complete µmBBN chip (**Figure 3A**) and endothelial coverage (**Figure 3B-D**) is shown. Endothelial barriers with high and low coverage are quantified to ascertain µmBBN chips are suitable for the addition of cancer cells (**Figure 3B**). Representative images of a

μmBBN chip with a confluent endothelial barrier that is acceptable for experimentation (**Figure 3C**) and a μmBBN chip with especially poor endothelial coverage that is not suitable for the addition of cancer cells are provided (**Figure 3D**). Long-term culturing of endothelial cells can result in coverage that spans beyond the membrane separating the top and bottom μmBBN chip chambers. Endothelial cells often grow both on top of and directly beneath the membrane, which does not affect cancer cell movement into the brain niche space but can make the plane fit difficult. Due to the variability of the μmBBN chip fabrication and endothelial coverage of the membrane, representative planes fit to a normal flat endothelial barrier (**Figure 3E**), and an atypical curved membrane are displayed for reference (**Figure 3F**). Drying the device in an oven at a temperature above 40 °C may cause a curved membrane as shown.

We observed phenotypic differences of the MDA-MB-231-BR-GFP and parental MDA-MB-231-GFP cell line when encountering astrocytic μmBBN that were quantified using the developed confocal tomographic analysis. The 4 phenotypic descriptors used for input into the machine learning algorithm (**Table 1**) are displayed in **Figure 4**.

Distance extravasated represents the distance in μm between the endothelial barrier and each cancer cell position in the μmBBN chip (**Figure 4A**). The endothelial barrier is located at 0 μm. Distances <0 μm represent cancer cells that remained in the flow chamber. Distances >0 μm indicate cancer cells that have extravasated through the endothelial barrier and entered the brain niche space. After 1-day of exposure to the μmBBN both MDA-MB-231-BR-GFP and MDA-MB-231-GFP were positioned within the endothelial barrier. However, after 2 and 9-Days of interaction a subset of the MDA-MB-231-BR-GFP migrated >100 μm into the astrocytic brain niche, whereas the parental MDA-MB-231-GFP cells remained in proximity to the endothelial barrier. We resolved the cancer cell positions at the endothelial barrier/brain niche interface by calculating the volume of each cancer cell that has passed through the endothelial barrier. The resulting percentage represents cancer cell extravasated by volume (**Figure 4B**). A 0% extravasated by cell volume indicates cancer cells that remain on top of the endothelial barrier, ranging to 100% when a cancer cell has completely extravasated through the endothelial barrier and resides in the brain niche space. The parental MDA-MB-231-GFP cells initially interact with the endothelial barrier after 1-Day of exposure to the μmBBN chip that were <50% extravasated by volume. At 2, and 9-Days the MDA-MB-231-GFP cells maintain a substantial proportion of cells that remained on top of the barrier away from the brain niche space. The MDA-MB-231-BR-GFP cells maintained a proportion of cells that were >100% extravasated, especially at the 2-Day timepoint.

The cancer cell shape changed dramatically over the duration of exposure to the μmBBN. Representative images of the cancer cells at each timepoint are depicted in **Figure 4C**. Morphological quantification of the cancer cell shape was calculated using sphericity, that accounts for cell volume and surface area (**Figure 4D**). The sphericity metric ranges from 0-1, with 1 representing a perfect sphere. Both MDA-MB-231-BR-GFP and MDA-MB-231-GFP cells were highly spherical 1-day post seeding into the μmBBN chip. After 2- and 9-days of interaction in the μmBBN chip, both cancer cell lines trended to decrease their spherical in shape, albeit at different rates. In addition to cancer cell shape, the volume in voxels of each cancer cell is also quantified

using the confocal tomographic analysis. Each cancer cell line was stratified into two groups in **Figure 4E-F**: "out", representing the cancer cells that transited through the endothelial barrier (>90% extravasated through the barrier) and "in", the population of cells that interact with the endothelial barrier but do not extravasate through (<90% extravasated). The cancer cell subpopulations that extravasated into the astrocytic niche were smaller in size compared to the cancer cells that remained in interaction with the endothelial barrier but did not fully extravasate through to the brain.

The brain-seeking MDA-MB-231-BR-GFP revealed a phenotypic pattern in the µmBBN chips distinct from the parental MDA-MB-231-GFP that can be exploited to differentiate between brain-metastatic and non-brain metastatic cancer cells using machine learning. The data was randomly separated into training and validation datasets to train the model and perform validation tests. To train the model, a total of 38,859 cells were used after filtering the data and the model was tested against 9,714 individual cells. The trained model was applied to the cancer cell lines and PDX-generated cancer cells that were analyzed in astrocytic µmBBN chips (4 isolated from patient brain metastases of a variety of primary tumor types, and 1 primary breast cancer tumor) to generate an index of brain metastatic probability (**Figure 5**). Eight different machine learning classification methods were tested: Naïve bayes, random forest, decision tree, *k*-nearest-neighbor (*k*NN), stochastic gradient descent, neural network, and Adaboost. The result of each method is shown in **Table 2**. Neural network and Adaboost were the 2 best performing classification methods that are recommended for use with data generated using the µmBBN platform with an AUC of 0.920 and 0.928, respectively. Moreover, they showed an accuracy of 0.833 and 0.853. The average of precision and recall (F1) for the Neural network and Adaboost methods were 0.847 and 0.860. From previous work where we applied this approach to PDX samples of non-metastatic breast tumor and known metastatic samples (breast, lung, ovarian, tongue) we found that the same approach applied to the PDX samples enabled accurate identification of the metastatic cells from the non-metastatic ones. **Table 2** shows the results for each machine learning algorithm applied to the PDX data wherein the same methods proved to be the most robust (Neural network and Adaboost (Random Forest). Of the 143 cells used in the testing set for the PDX samples, 71 were non-metastatic, 46 were metastatic breast, 11 were metastatic tongue, 13 were metastatic lung and 2 were metastatic ovarian. Each cell type produced an overall accuracy of 0.88 but individual had the following approximate accuracies: non-metastatic breast: 0.96, metastatic breast: 0.80, metastatic tongue: 0.80, metastatic lung: 0.92, metastatic ovarian: 1.0

FIGURE AND TABLE LEGENDS:

Figure 1: Experimental workflow. (**A**) Schematic representation of the microfluidic device assembly process. A spinner is used to deposit a thin film of PDMS:toluene glue onto a 50 mm x 75 mm glass slide. Each half of the µmBBN device is stamped channel side facing the glue and then assembled with a polycarbonate membrane (5 µm pores) between the µmBBN device parts. The µmBBN devices are placed in a 37 °C oven for 24 h to cure the glue. Devices are then dried in a vacuum desiccator for at least 48 h prior to experimental use. A µmBBN device and 50 mm x 75 mm glass slide are activated with a plasma treatment and bonded together. Standard P200

pipettes cut at the tips are inserted into all µmBBN device inlets and outlets. The completed µmBBN device is then sterilized by an 8 min (200 W) plasma treatment then transferred to a sterile secondary container. (**B**) Schematic overview of utilizing the microfluidic device scaffolding to create a cellular blood brain barrier and brain niche micro-environment. Inside a biosafety cabinet, a mixture of astrocytes in collagen are seeded into the bottom µmBBN device chamber and allowed to solidify for 1 h at 37 °C. Matrigel is used to coat the membrane through the top flow chamber for 1 h at 37 °C. Then endothelial cells are seeded into one tip of the top chamber and allowed to flow and settle for 15 min. This seeding is repeated x4, alternating sides of the flow chamber.

Figure 2: Confocal tomographic analysis overview. The software begins by converting a microscopic confocal Z-stack image into a 3-D model of the cells using segmentation and 3D meshes. The program then calculates the center position of each cell (centroid) and fits a plane to the endothelial barrier. Phenotypic measurements of each single cell are then tabulated.

Figure 3: Endothelial barrier coverage and plane fitting. (**A**) Representative schematic and image of a µmBBN device. The dashed white line within the top view schematic indicates the area of the device represented in the cross-sectional view. (**B**) Comparison of high and low endothelial coverage of µmBBN devices prior to the application of cancer cells. Welch two-sample t-test, *** $p < 0.1*10^{-4}$. (**C**) Representative image of high endothelial coverage. The dashed white box within the inset schematic of a µmBBN device indicates the location of the endothelial cells within the device. Scale bars of overview and inset images = 200 µm. (**D**) Representative image of low endothelial coverage. Scale bars of overview and inset images = 200 µm. (**E**) Example plane fit of a flat endothelial barrier. The green rectangle represents the position of the endothelial plane. Dots represent single endothelial cells comprising the barrier. Yellow dots are endothelial cells above the plane, and purple dots are cells that fall below the plane. Endothelial cells above the plane (yellow dots) exhibit a tendency to grow up the sidewalls and top of the device to form a tube. (**F**) Example plane fit of a µmBBN device with a curved plane.

Figure 4: Quantification of cellular phenotypes of brain-metastatic and parental cell phenotypes in astrocytic blood brain niche microfluidic chips. (**A**) Strip plot of distance in µm of cancer cells from the endothelial barrier at 1, 2, and 9-Days. The dashed black line at 0 µm represents the endothelial barrier. Red boxes indicate a subset of MDA-MB-231-BR-GFP cells that migrated far into the brain niche. (**B**) Violin plot of the percent total volume of cancer cells extravasated through the endothelial barrier at 1, 2, and 9-Days. Short dashed lines represent quartiles, longer dashed line represents the mean. (**C**) Representative images of the morphology of cancer cells in µmBBN device. Scale bar = 25 µm. (**D**) Violin plot of the sphericity of cancer cells in µmBBN device at 1, 2, and 9-Days. Sphericity ranges from 1: spherical to 0: not spherical. (**E**) Box plot of MDA-MB-231-GFP cell volume in the µmBBN device in voxels for cells resting outside the endothelial barrier (out) and cells that extravasated through the barrier (in). (**F**) Box plot of MDA-MB-231-BR-GFP cell volume in the µmBBN device in voxels for cells resting outside the endothelial barrier (out) and cells that extravasated through the barrier (in). The box displays the quartiles and whiskers extend to show the proportion of the interquartile range past the low and high quartiles. Pairwise Wilcoxon Rank Sum and Kruskal-Wallis with Dunn's multiple

comparisons, *** $p < 0.1*10^{-4}$. Reproduced from reference[24] with permission from the Royal Society of Chemistry.

Figure 5: Representative results of machine learning classification of cancer cells. (**A**) Machine learning overview. Demonstrates process of splitting data collected from confocal tomography, filtering the data, training the machine learning algorithm using 10-fold validation and then testing the model against a random sample of 20% of the data the was reserved. The selected model can then be applied on new data to collect the metastatic index of individual cells. (**B**) ROC curves showing the performance of 8 different machine learning algorithms for MDA-231-BR-GFP and MDA-231-GFP cells culture for 1, 2 and 9-Days before imaging. This is representative of the type of curve to be analyzed to understand the performance of the trained model. (**C**) ROC curves for 8 different machine learning algorithms applied to patient derived xenograft (PDX) dissociated cells cultured for 2-Days. This is representative of the type of curve to be analyzed to understand the performance of the trained model. Reproduced from reference[24] with permission from the Royal Society of Chemistry.

Table 1: List of descriptors by feature type. The phenotypic characterization of tumor cells is represented using a panel of descriptors. The red box indicates the descriptors that have been used to predict brain metastatic probability via machine learning.

Table 2: Comparison of machine learning methods to classify cancer cells and PDX cancer cells by brain metastatic potential.

DISCUSSION:

We have developed and presented a new method that adapts tools often utilized in clinical imaging analyses for measurement of extravasation and migration of cancer cells through an endothelial barrier into brain tissue. We pose this approach can be useful for both in vivo and in vitro measurements; we have demonstrated its use on a 3D microfluidic system recapitulating brain vasculature. Cancer cell measurements including distance extravasated, percent extravasated by volume, sphericity, and volume are quantified using this technique. Distance extravasated and percent extravasated by volume permit the user to reconstruct the position of the cancer cells within the chip to assess extravasation across the barrier and migration within the tissue. Cell shape measurements such as sphericity and volume are related to the dynamic movements or function of the cell at each timepoint. Migratory MDA-MB-231-BR-GFP cells exhibit a high level of sphericity when initially introduced into the µmBBN device and become less spherical in shape as they decrease their movement and begin to colonize the niche. Overall cell volume of the MDA-MB-231-GFP and MDA-MB-231-BR-GFP differed due to the difference in shape of the cell lines. Cancer cells that cross the endothelial barrier are more rounded than the cells that do not traverse through the barrier, thus smaller round cells may be able to extravasate across the endothelial layer more efficiently.

Two critical steps exist within the protocol that facilitate success. The first occurs during the assembly of the µmBBN device upper and lower parts that are separated by the porous membrane. Upper and lower device parts must be mated so that the inlets and outlets overlap

but are not occluded by the membrane in between to promote proper flow. All µmBBN devices with poor mating of the upper and lower device parts or membrane alignment are discarded to minimize fluctuations in quality. Subsequent baking to cure the PDMS:toluene glue to assemble the device is critical to perform at 37 °C to produce µmBBN devices with membranes that are flat. Baking temperatures that exceed 37 °C tend to produce devices with a curved membrane that makes image analysis difficult, especially when fitting a plane to the endothelial barrier. The second critical step happens during the seeding of the endothelial barrier. Seedings should occur at a minimum of fifteen minute intervals between the two inlets feeding the top part of the device to ensure random distribution of the endothelial cells onto the membrane of the device. Seeding of the collagen mixture containing astrocytes into the chip may require troubleshooting and modification to the lab-specific protocol. If the membrane surface of the device is not hydrophobic, the collagen will fill both the bottom and top parts of the device and set so that it clogs all flow through the top part of the device. The purpose of the final plasma gas treatment is to make the device surface hydrophobic. In this case, we recommend adjustment of the plasma gas treatment of the device to increase hydrophobicity.

We have observed some limitations with this approach. For example, the approach used to induce cell fluorescence can impact the imaging quality. When using live cell tracking dyes, the fluorescent pattern is made of small spots, while transfected or transduced expression of fluorophores produces a uniform pattern. The spotty pattern requires additional and sometimes error prone clustering of pixels. Additionally, the sensitivity of the measurement is dependent on the care taken during imaging. Higher resolution images and more z slices improves resolution, but also takes more time to image and analyze. Cells that are touching can also be incorrectly analyzed as a large single cell. This is a problem for many automated imaging systems but can be addressed in two ways. The first is that the endothelial layer has many cells touching, but their combination has negligible impact on the final location of the cutting plane. The second is the number of cancer cells is low enough that it is rare they are touching. Errors introduced when fitting the plane can occur for several reasons. The first is that some endothelial cells may have migrated away from the central membrane during cell culture. This can result in endothelial cells coating the entire channel or invading the collagen filled space, thereby skewing the measurement. Another source of error is, paradoxically, the manual adjusting of the plane to fix the previous error. However, repeatability and reproducibility studies have found this to have minimal impact. Finally, we observed that under certain circumstances the Boolean cutting of the cell mesh may fail or the algorithm to close the cut mesh may also fail. The techniques used here are the current “state of the art”, and these problems are currently being addressed by algorithmic scientists.

The results from training the machine learning algorithms (AI) against data collected by confocal tomography of the µmBBN demonstrate that the considerable number of individual cells analyzed by this approach may help address issues of capturing heterogeneity found in cancer cells. An AUC greater than 0.9 is considered a high performing classifier. Here we demonstrated an AUC of 0.928. We expect that as the method is improved upon performance will continue to increase. As with all AI methods, care must be taken to select the training data set carefully so that it represents broadly the type of data expected to be tested against. For this reason, we may

expect that the performance would degrade, if the model were applied directly to patient samples for example without first exposing the model to a robust collection of patient samples. We demonstrate this here to some extent by including 1-Day, 2-Day, and 9-Day measurements for the cancer cells in the model compared to the 2-Day day used for the previous work. We observe that the broad sampling reduces the performance of the model slightly and shows how sensitive some of the poorer performing methods may be, thus suggesting that users may want to test several models on their data. **Table 2** describing PDX results shows an overall good performance. However, individual PDX types demonstrate that the proportion of cells measured from each sample differ and may influence the performance for each site of origin. For example, the ovarian sample only produced two cells for the testing set. In contrast, metastatic breast cancer which had a larger population. This data set was intended to demonstrate that the cells survive in the niche and can be analyzed, but also highlights interpretive care is needed. Alterations to the target variable may also guide researchers in identifying sub-clones with other traits such as interactions with stromal cells or quiescent behavior.

This approach is important as more labs adopt membrane on-a-chip systems such as blood brain barrier on a chip, lung on a chip and gut on a chip[11,42]. The majority of these chips are assembled so that the membrane is parallel with the imaging system, which until now it has meant that it would be difficult to measure when and how many cells have moved from one side of the membrane to the other[15,28]. Moreover, when compared to horizontally oriented chips, vertically oriented chips provide a much larger membrane area increasing the dynamic range of the experiment. In addition, because orientation of the membrane is not critical for this analysis technique, confocal tomography could potentially enable new *in vitro* experiments. For instance, imaging the extravasation of breast cancer cells from the murine fat pad into the blood stream would be approachable by these methods. This could help researchers identify how the cancer cells probe the interface between the breast ECM and vessel.

In conclusion, we presented a methodology to construct a 3D microfluidic device that recapitulates the blood brain niche and demonstrate how to use confocal tomography and machine learning for analysis. Using this platform, we identified brain-metastatic cancer cell characteristics that differentiate between brain metastatic and non-metastatic PDX cancer cells based on their behavior within the µmBBN device. Future work will improve the clinical applicability of this platform as a diagnostic towards predicting brain metastases. We believe that having presented this platform will be useful and interesting to labs which need to measure cells of any type migrating or extravasating across a membrane. This is of importance as pre-clinical models of the tumor micro-environment become increasingly sophisticated so to must the engineering of the models and supporting software. To aid in robust analysis of the data we have packaged this tool as a simple to use, shared python notebook with installation instructions[30].

ACKNOWLEDGMENTS:
We thank the Steeg Lab, at the National Cancer Institute for the generous donation of MDA-MB-231-BR-GFP cells. Confocal microscopy was performed at the University of Michigan Biointerfaces Institute (BI). Flow cytometry was performed at the University of Michigan Flow Cytometry Core. Viral vectors were created by the University of Michigan Vector Core. We also

thank Kelley Kidwell for guidance in statistical analysis of these data.

FUNDING:

C.R.O. was partially supported by an NIH T-32 Training Fellowship (T32CA009676) and 1R21CA245597-01. T.M.W. was partially supported by 1R21CA245597-01 and the National Center for Advancing Translational Sciences of the National Institutes of Health under Award Number UL1TR002240. Funding for materials and characterization was provided by National Cancer Institute of the National Institutes of Health under award number 1R21CA245597-01, P30CA046592, 5T32CA009676-23, CA196018, AI116482, METAvivor Foundation, and the Breast Cancer Research Foundation. The content is solely the responsibility of the authors and does not necessarily represent the official views of the National Institutes of Health

DISCLOSURES:

There are no disclosures to declare.

REFERENCES:

1 Rastogi, K. et al. Palliation of Brain Metastases: Analysis of Prognostic Factors Affecting Overall Survival. *Indian Journal of Palliative Care.* **24** (3), 308-312 (2018).

2 Wang, R. et al. The Clinicopathological features and survival outcomes of patients with different metastatic sites in stage IV breast cancer. *BMC Cancer.* **19** (1), 1091 (2019).

3 Valster, A. et al. Cell migration and invasion assays. *Methods.* **37** (2), 208-215 (2005).

4 Eccles, S. A., Box, C., Court, W. Cell migration/invasion assays and their application in cancer drug discovery. *Biotechnology Annual Review.* **11**, 391-421 (2005).

5 Brekhman, V., Neufeld, G. A novel asymmetric 3D in-vitro assay for the study of tumor cell invasion. *BMC Cancer.* **9** 415 (2009).

6 Chen, H. C. Boyden chamber assay. *Methods in Molecular Biology.* **294**, 15-22 (2005).

7 Poissonnier, A., Legembre, P. Boyden Chamber Assay to Study of Cell Migration Induced by Metalloprotease Cleaved-CD95L. *Methods in Molecular Biology.* **1557**, 117-123 (2017).

8 Li, X., Yang, H., Huang, H., Zhu, T. CELLCOUNTER: novel open-source software for counting cell migration and invasion in vitro. *BioMed Research International.* **2014**, 863564 (2014).

9 Little, A. C. et al. IL-4/IL-13 Stimulated Macrophages Enhance Breast Cancer Invasion Via Rho-GTPase Regulation of Synergistic VEGF/CCL-18 Signaling. *Frontiers in Oncology.* **9**, 456 (2019).

10 Allen, S. G. et al. Macrophages Enhance Migration in Inflammatory Breast Cancer Cells via RhoC GTPase Signaling. *Scientific Reports.* **6**, 39190 (2016).

11 Bhatia, S. N., Ingber, D. E. Microfluidic organs-on-chips. *Nature Biotechnology.* **32** (8), 760-772 (2014).

12 Huh, D. et al. Reconstituting organ-level lung functions on a chip. *Science.* **328** (5986), 1662-1668 (2010).

13 Chen, Y. C. et al. Single-cell Migration Chip for Chemotaxis-based Microfluidic Selection of Heterogeneous Cell Populations. *Scientific Reports.* **5**, 9980 (2015).

14 Choi, Y. P. et al. Cancer-associated fibroblast promote transmigration through endothelial brain cells in three-dimensional in vitro models. *International Journal of Cancer.* **135** (9), 2024-2033 (2014).

15 Takeshita, Y. et al. An in vitro blood-brain barrier model combining shear stress and endothelial cell/astrocyte co-culture. *Journal of Neuroscience Methods.* **232**, 165-172 (2014).
16 Kienast, Y. et al. Real-time imaging reveals the single steps of brain metastasis formation. *Nature Medicine.* **16** (1), 116-122 (2010).
17 Schroeder, W., Martin, K., Lorenson, B. *The Visualization Toolkit*. 4th edn (Kitware, 2006).
18 Wells, W. M., Grimson, W. L., Kikinis, R., Jolesz, F. A. Adaptive segmentation of MRI data. *IEEE Transactions on Medical Imaging.* **15** (4), 429-442 (1996).
19 Agarwal, S. K., Singh, S., Ghuman, S. S., Sharma, S., Lahiri, A. K. Radiological assessment of the Indian children with congenital sensorineural hearing loss. *International Journal of Otolaryngology.* **2014**, 808759 (2014).
20 Mansfield, P., Maudsley, A. A. Medical imaging by NMR. *The British Journal of Radiology.* **50** (591), 188-194 (1977).
21 Plewes, D. B., Kucharczyk, W. Physics of MRI: a primer. *Journal of Magnetic Resonance Imaging.* **35** (5), 1038-1054 (2012).
22 Batteux, C., Haidar, M. A., Bonnet, D. 3D-Printed Models for Surgical Planning in Complex Congenital Heart Diseases: A Systematic Review. *Frontiers in Pediatrics.* **7**, 23 (2019).
23 Thibault, F. et al. MRI for surgical planning in patients with breast cancer who undergo preoperative chemotherapy. *American Journal of Roentgenology.* **183** (4), 1159-1168 (2004).
24 Oliver, C. R. et al. A platform for artificial intelligence based identification of the extravasation potential of cancer cells into the brain metastatic niche. *Lab on a Chip.* **19** (7), 1162-1173 (2019).
25 Gril, B. et al. Reactive astrocytic S1P3 signaling modulates the blood-tumor barrier in brain metastases. *Nature Communications.* **9** (1), 2705 (2018).
26 Badilescu, S., Packirisamy, M. *BioMEMS: Science And Engineering Perspectives*. (Taylor & Francis/CRC Press, 2011).
27 Liu, C. *Foundations of MEMS*. 2nd edn (Prentice Hall, 2012).
28 Booth, R., Kim, H. Characterization of a microfluidic in vitro model of the blood-brain barrier (muBBB). *Lab on a Chip.* **12** (10), 1784-1792 (2012).
29 Lockman, P. R. et al. Heterogeneous blood-tumor barrier permeability determines drug efficacy in experimental brain metastases of breast cancer. *Clinical Cancer Research.* **16** (23), 5664-5678 (2010).
30 C. Ryan Oliver, T. M. W. Con-tom: A Jupyter Notebook for Analyzing the tumor micro-environment in confocal images. *Zenodo.* http://doi.org/10.5281/zenodo.3825719 (Version 0.8), 3825719 (2020).
31 Lorensen, W. E., Johnson, C., Kasik, D., Whitton, M. C. History of the Marching Cubes Algorithm. *IEEE Computer Graphics and Applications.* **40** (2), 8-15 (2020).
32 Kleinbaum, D. G., Kupper, L. L. *Applied regression analysis and other multivariable methods*. (Duxbury Press, 1978).
33 Berg, M. d. *Computational geometry : algorithms and applications*. 2nd, rev. edn (Springer, 2000).
34 Esch, M. B., Post, D. J., Shuler, M. L., Stokol, T. Characterization of in vitro endothelial linings grown within microfluidic channels. *Tissue Engineering Part A.* **17** (23-24), 2965-2971 (2011).
35 Brinkley, B. R. et al. Variations in cell form and cytoskeleton in human breast carcinoma

cells in vitro. *Cancer Research.* **40** (9), 3118-3129 (1980).
36 Eigenmann, D. E. et al. Comparative study of four immortalized human brain capillary endothelial cell lines, hCMEC/D3, hBMEC, TY10, and BB19, and optimization of culture conditions, for an in vitro blood-brain barrier model for drug permeability studies. *Fluids and Barriers of the Central Nervous System.* **10** (1), 33 (2013).
37 Griep, L. M. et al. BBB on chip: microfluidic platform to mechanically and biochemically modulate blood-brain barrier function. *Biomedical Microdevices.* **15** (1), 145-150 (2013).
38 Weksler, B., Romero, I. A., Couraud, P. O. The hCMEC/D3 cell line as a model of the human blood brain barrier. *Fluids and Barriers of the Central Nervous System.* **10** (1), 16 (2013).
39 Dello Russo, C. et al. The human microglial HMC3 cell line: where do we stand? A systematic literature review. *Journal of Neuroinflammation.* **15** (1), 259 (2018).
40 Dun, M. D. et al. Proteotranscriptomic Profiling of 231-BR Breast Cancer Cells: Identification of Potential Biomarkers and Therapeutic Targets for Brain Metastasis. *Molecular & Cellular Proteomics.* **14** (9), 2316-2330 (2015).
41 Xing, F. et al. Reactive astrocytes promote the metastatic growth of breast cancer stem-like cells by activating Notch signalling in brain. *EMBO Molecular Medicine.* **5** (3), 384-396 (2013).
42 Zhang, B., Radisic, M. Organ-on-a-chip devices advance to market. *Lab on a Chip.* **17** (14), 2395-2420 (2017).

Figure 1

Click here to access/download;Figure;Figure_1.pdf

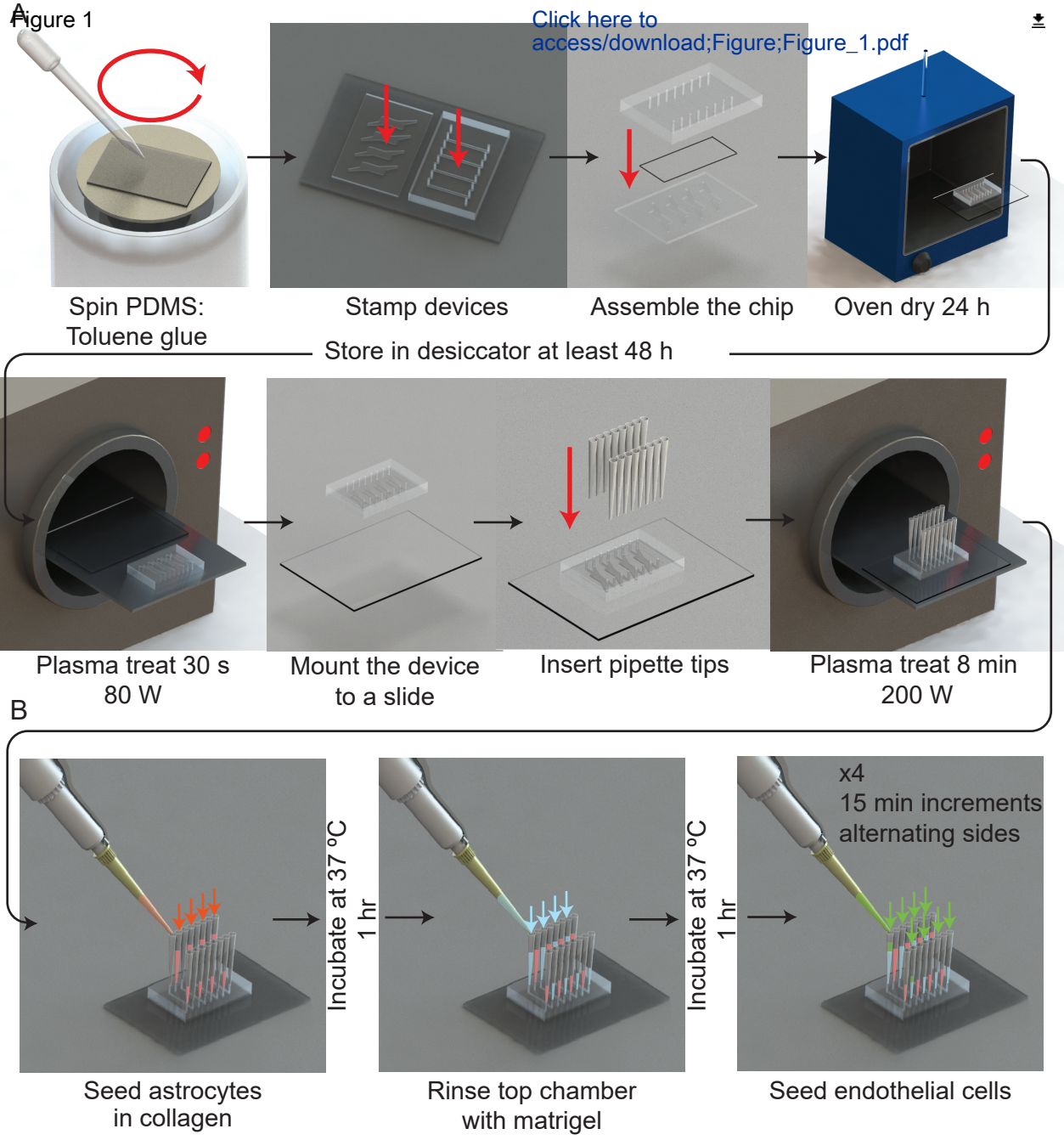

Figure 2

Click here to access/download;Figure;Figure_2.pdf

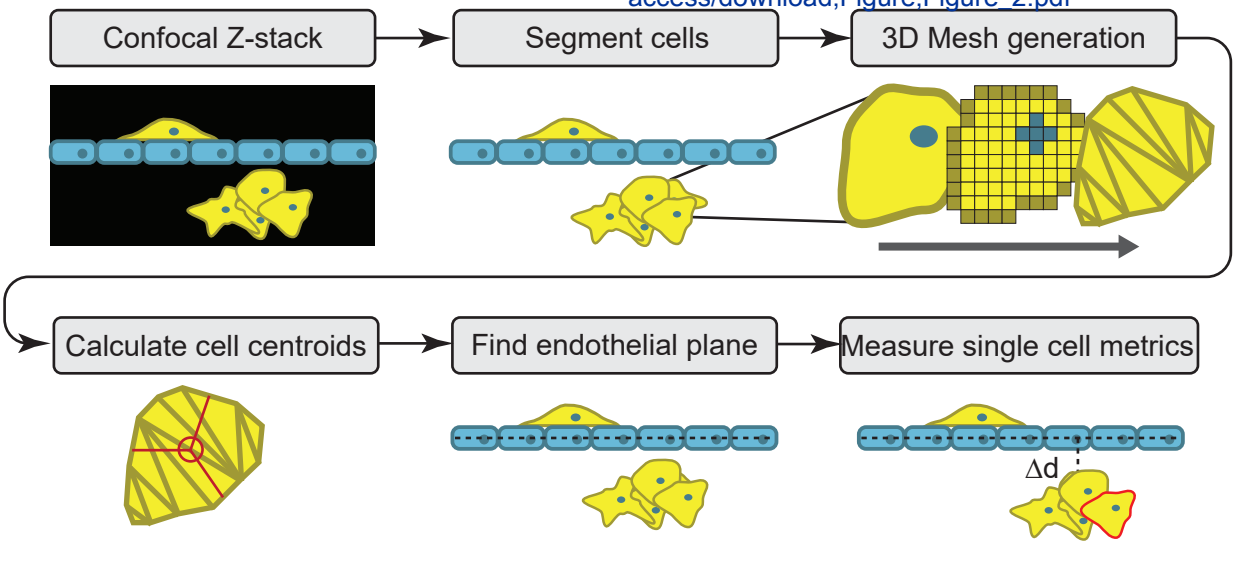

Figure 3

Click here to access/download;Figure;Figure_3.pdf

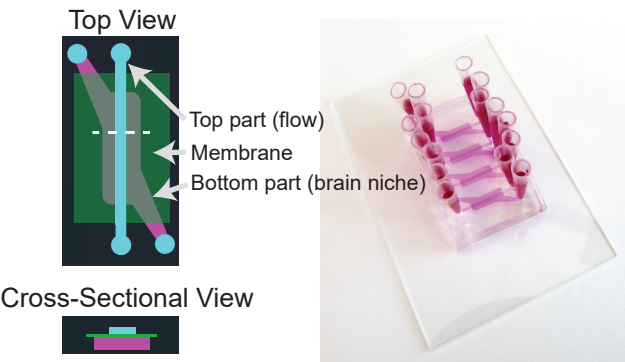

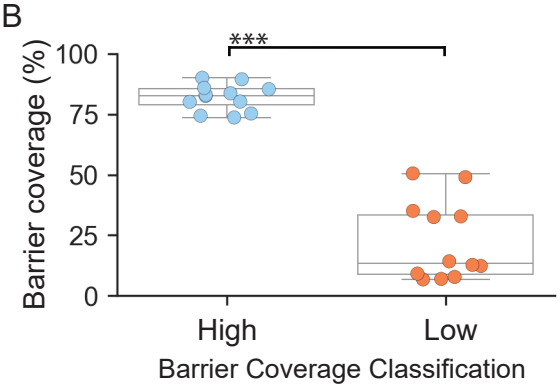

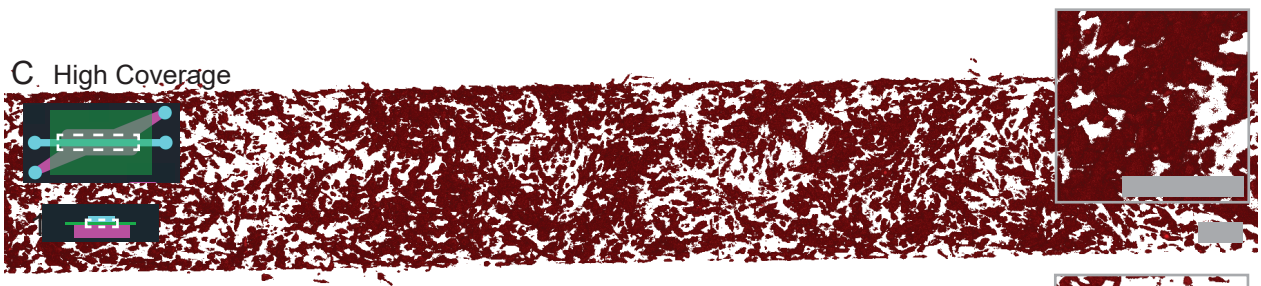

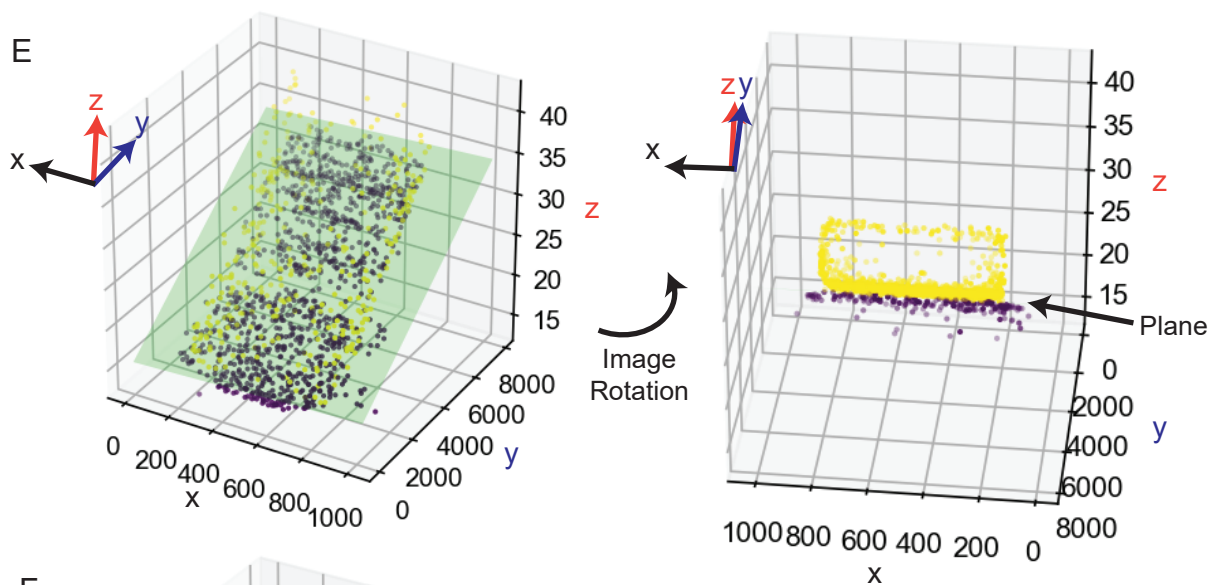

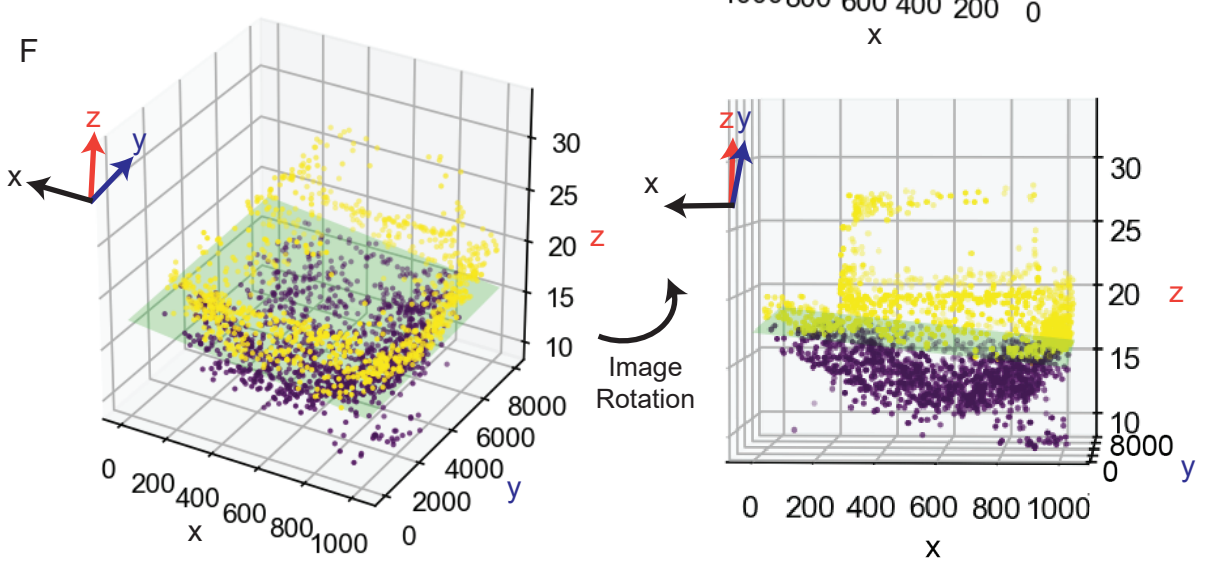

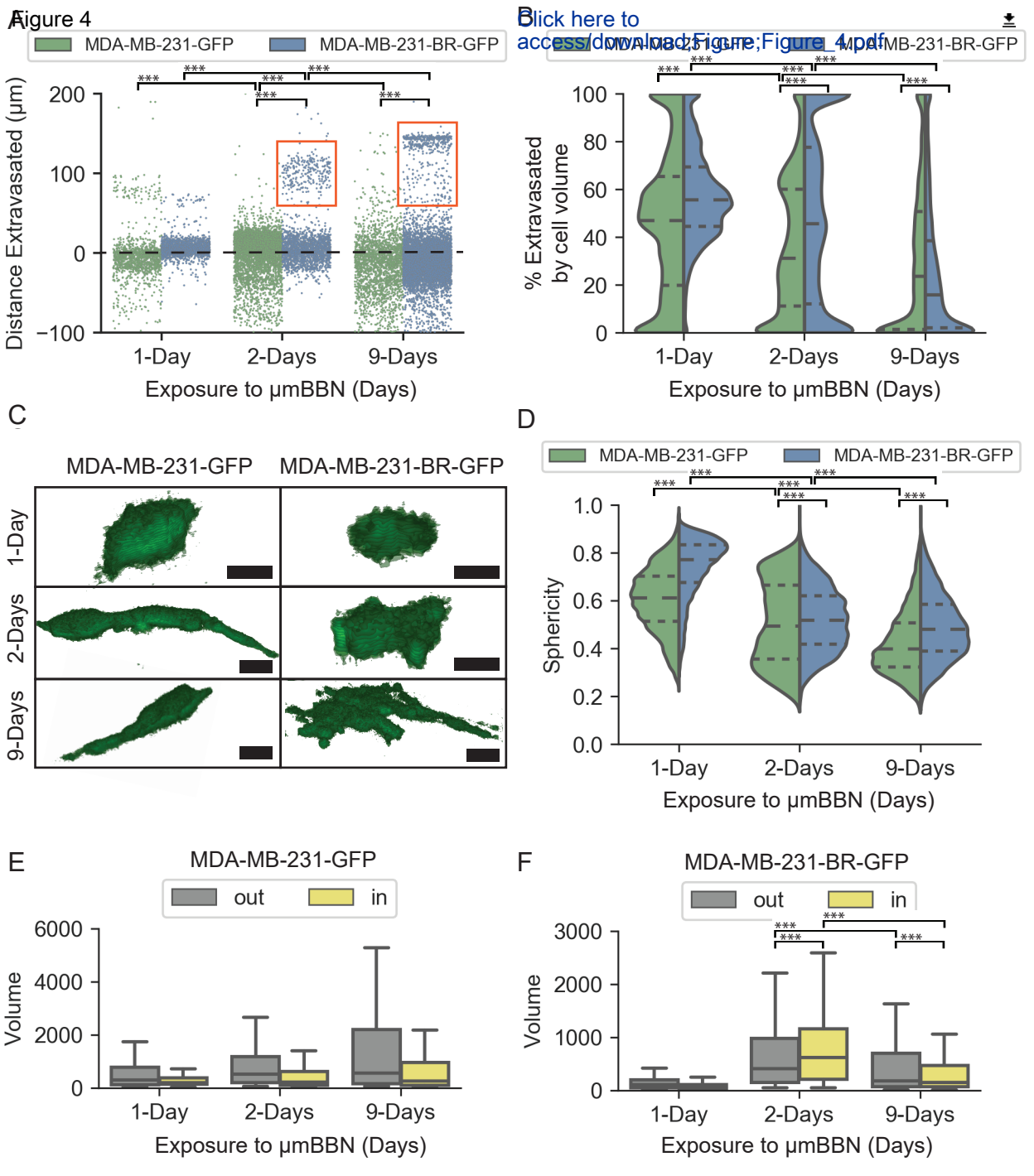

Figure 5

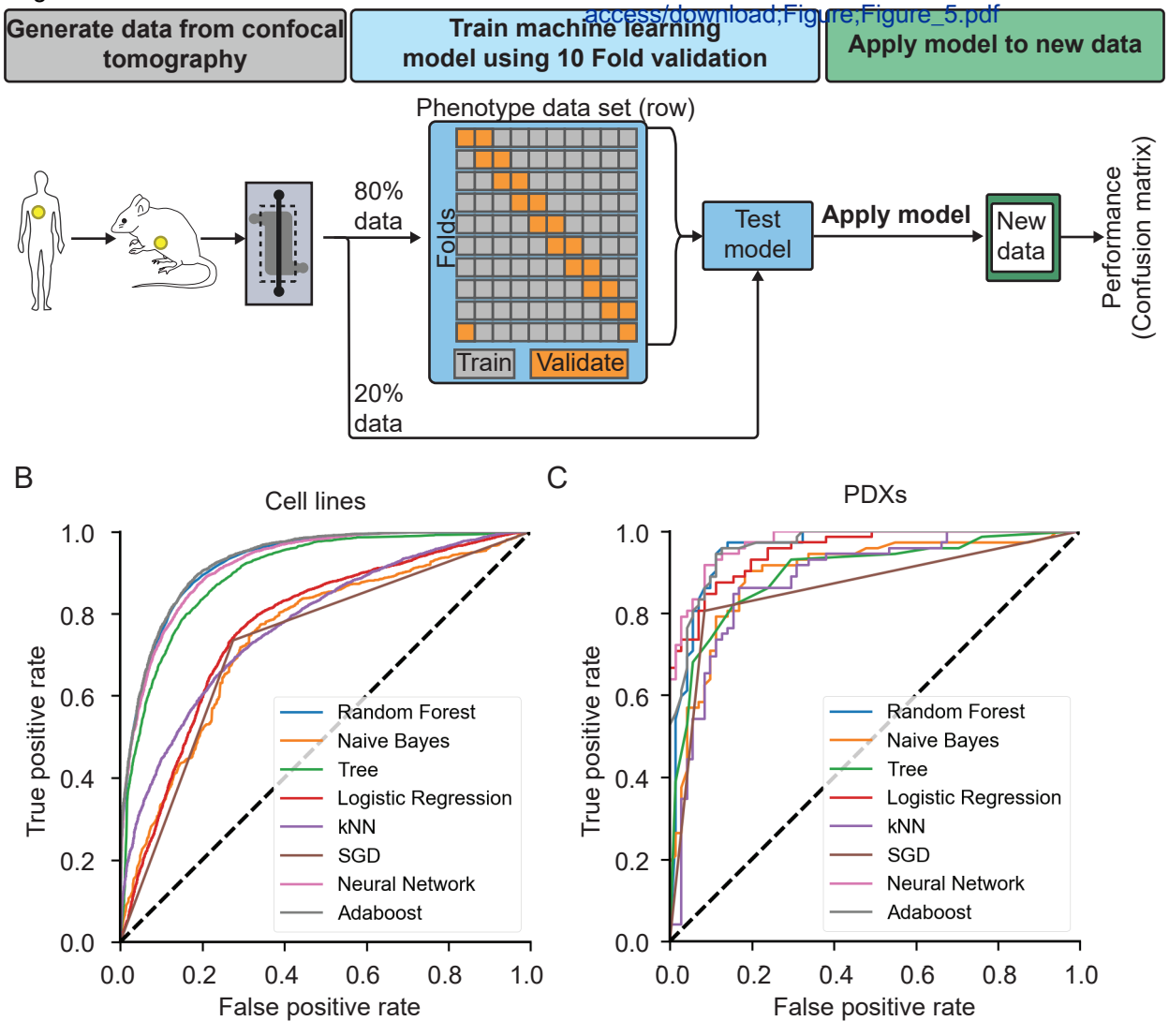

Table 1

Feature	Descriptor
Tumor cell	% extravasated into the niche
Tumor cell	Volume
Tumor cell	Sphericity
Tumor cell	Distance extravasated
Tumor cell	Live cell 2D migration
Micro-metastasis	Porosity
Micro-metastasis	Stromal interaction
Micro-metastasis	Age
Micro-metastasis	Growth rate
Stromal cell	Volume
Stromal cell	Distance from nearby cancer cells
Stromal cell	Distance from endothelial barrier
Stromal cell	Shape

Table 2

Cancer cells			
Method	AUC	Accuracy	F1
Neural Network	0.925	0.84	0.847
AdaBoost	0.928	0.853	0.86
Random Forest	0.925	0.849	0.855
Decision Tree	0.898	0.817	0.827
kNN	0.775	0.702	0.718
Logistic Regression	0.769	0.735	0.751
Naïve Bayes	0.745	0.715	0.73
SGD	0.73	0.73	0.737

PDX Cancer cells			
Method	AUC	CA	F1
Neural Network	0.972	0.881	0.878
Random Forest	0.964	0.888	0.887
AdaBoost	0.957	0.881	0.879
Tree	0.954	0.867	0.865
Logistic Regression	0.897	0.832	0.831
Naïve Bayes	0.896	0.846	0.849
kNN	0.882	0.818	0.814
SGD	0.861	0.86	0.853

Name of Material/Equipment	Company	Catalog Number
0.25% Trypsin-EDTA with phenol red	Thermo Fisher Scientific	25200056
1.5 mm biopsy punch with plunger	Integra LifeSciences Corporation	33-31A-P/25
10x MEM	Thermo Fisher Scientific	11430030
150 mm petri dishes	Fisher Scientific	FB0875714
1x DPBS, without Ca and Mg	Thermo Fisher Scientific	14190144
200uL pipette tip	Fisher Scientific	02-707-411
4 inch silicon wafer	University Wafer	452
48 mm wide packing tape	Fisher Scientific	19-072-097
50 x 75 mm glass slide	Fisher Scientific	12-550C
A1 confocal microscope	Nikon	
acetone	Fisher Scientific	A9-20
antibiotic/antimycotic (penicillin/streptomycin/amphotericin)	Gibco	15240062
box cutter blade	Fisher Scientific	NC1721575
dissection scissors	Fisher Scientific	08-951-5
DMEM with 4.5 g/L glucose	Thermo Fisher Scientific	11960-044
double sided tape	Fisher Scientific	NC0879005
EGM-2	Lonza	CC-3162
Fetal Bovine Serum, Heat inactivated	Corning	MT35011CV
Fiji software	ImageJ	
glass vial	Fisher Scientific	03-341-25D
glutamax	Thermo Fisher Scientific	35050061
hCMEC/D3	EMD Millipore	SCC066
Jupyter notebook	Anaconda	
L-glutamine	Thermo Fisher Scientific	25030081
Matrigel - growth factor reduced with phenol red	Corning	CB-40230A
MDA-MB-231	ATCC	HTB-26
MDA-MB-231-BR-GFP	Dr. Patricia Steeg, NIH	
N-2 growth supplement	Thermo Fisher Scientific	17502048
normal human astrocytes (NHA)	Lonza	CC-2565
Orange software	University of Ljubljana	

Pasteur pipette	Fisher Scientific	13-711-9AM
Photolithography masks	Photosciences Incorporated	
pLL3.7-dsRed	University of Michigan Vector Core	
pLL-EV-GFP	University of Michigan Vector Core	
pLOX-TERT-iresTK	Addgene	12245
pMD2.G	Addgene	12259
polycarbonate membrane, 5um pore size	Millipore	TMTP04700
psPAX2	Addgene	12260
PureCol, 3 mg/mL	Advanced Biomatrix	5005
sodium bicarbonate	Thermo Fisher Scientific	25080094
sodium pyruvate	Thermo Fisher Scientific	11360070
Solo cup	Fisher Scientific	NC1416545
SU-8 2075	MicroChem Corporation	Y111074 0500L1GL
SU8 developer	MicroChem Corporation	Y020100 4000L1PE
Sylgard 184	Ellsworth Adhesive Company	NC0162601
Toluene	Sigma-Aldrich	179965-1L
Tricholoro perfluoro octyl silane	Sigma-Aldrich	448931-10G

Comments/Description

Type I bovine collagen

Editorial Comments:

Please take this opportunity to thoroughly proofread the manuscript to ensure that there are no spelling or grammatical errors.

• *Protocol Detail:*

1) Please use the imperative voice for ALL steps.

2) Please note that your protocol will be used to generate the script for the video, and must contain everything that you would like shown in the video. Please add more specific details (e.g. button clicks for software actions, numerical values for settings, etc) to your protocol steps. There should be enough detail in each step to supplement the actions seen in the video so that viewers can easily replicate the protocol.

• *Protocol Numbering:* all steps should be lined up at the left margin with no indentations. There must also be a one-line space between each protocol step.

• *Protocol Highlight:* After you have made all of the recommended changes to your protocol (listed above), please re-evaluate the length of your protocol section. There is a 10-page limit for the protocol text, and a 3- page limit for filmable content. If your protocol is longer than 3 pages, please highlight ~2.5 pages or less of text (which includes headings and spaces) in yellow, to identify which steps should be visualized to tell the most cohesive story of your protocol steps.

1) The highlighting must include all relevant details that are required to perform the step. For example, if step 2.5 is highlighted for filming and the details of how to perform the step are given in steps 2.5.1 and 2.5.2, then the sub-steps where the details are provided must be included in the highlighting.

2) The highlighted steps should form a cohesive narrative, that is, there must be a logical flow from one highlighted step to the next.

3) Please highlight complete sentences (not parts of sentences). Include sub-headings and spaces when calculating the final highlighted length.

4) Notes cannot be filmed and should be excluded from highlighting.

• *Discussion:* JoVE articles are focused on the methods and the protocol, thus the discussion should be similarly focused. Please ensure that the discussion covers the following in detail and in paragraph form (3-6 paragraphs): 1) modifications and troubleshooting, 2) limitations of the technique, 3) significance with respect to existing methods, 4) future applications and 5) critical steps within the protocol.

• *References:* Please spell out journal names.

If your figures and tables are original and not published previously or you have already obtained figure permissions, please ignore this comment. If you are re-using figures from a previous publication, you must obtain explicit permission to re-use the figure from the previous publisher (this can be in the form of a letter from an editor or a link to the editorial policies that allows you to re-publish the figure). Please upload the text of the re-print permission (may be copied and pasted from an email/website) as a Word document to the Editorial Manager site in the "Supplemental files (as requested by JoVE)" section.

Please also cite the figure appropriately in the figure legend, i.e. "This figure has been modified from [citation]."

Comments from Peer-Reviewers:

Reviewer #1:

Manuscript Summary:

Thanks to authors for sharing their work on this important subject in the form of methods paper.

Major Concerns:

Authors need to revise their work to have a text that flows in appropriate manner and using correct tense of the verbs. The MS swishes between the use of present and past tense which creates some confusion. Most of these sections are presented like a recipe which are good for reader and user to follow. However other sections need to be revised, e.g. Sections 3.1., 4.3, 7.2 and 8.3 to mention some examples. Authors need to carefully revise this throughout the MS.

Conclusion section should be rewritten to be clear and includes relevant information derived from the study/developed method.

Minor Concerns:

Abstract:

"3D models of brain" start sentences with words and not numbers.

Introduction:

"3D structures" write in full, abbreviated words of 3D. Once this is done use abbreviation subsequently, e.g. to replace the full words in "three-dimensional tools" in the second para of the intro sections. Revise all abbreviations and their subsequent use in the MS.

Correct "Independently of migration" to "Independent of migration"

Protocol:

You may consider changing "made of two sides" to "made of two parts"

Correct "Tricholoro perfluoroctyl" to "Trichloro perfluorooctyl"

Revise the following sentence for clarity "An alternative is to fabricate an aluminum mold the wafer sits inside of to improve flatness and reduce downstream confocal imaging time."

What is the average pore size in the polycarbonate membrane?

You may consider changing "experimental terminus"

In section 7.2. instead of citing paper Doi cite as a regular reference

Reviewer #2:

Manuscript Summary:

This is a good manuscript on an implementation to study cellular responses during brain metastasis on blood brain niche using 3D in vitro microfluidic tumor microenvironment model and machine learning technique.

Major Concerns:

Although the authors demonstrated the claim for the novelty of this approach used in the manuscript and showed scientific research in the manuscript, the rationales for the approach are not quite convincing to be published in Journal of Visualized Experiments since there are some experimental designs that need more clarification to rationalize the approach.

Minor Concerns:

Here are some issues that can help improve this manuscript.

1. It is necessary to more convincingly emphasize why the astrocytic microenvironment should be constructed to recapitulate blood brain niche in terms of physiological relevance.

2. It should be addressed why the measurement of sphericity is important to understand metastatic tumor traits.

3. Figure 3A, there should be more detailed indications for cross-section and top view scheme for this device.

4. Figure 3B, it is necessary to add an axis title to the horizontal axis in the chart, where high and low mean endothelial coverage of μmBBN devices.

5. Figure 3C and 3D, there should be an additional scheme for the platform to indicate the location of the endothelial cells layer in the platform.

6. Figure 3C, it is necessary to demonstrate the representative confocal image, which shows proteins to mark barrier structures such as ZO-1 for a confluent endothelial barrier condition.

7. Figure 4, there should be testing of the statistical significance of results for all graphs.

8. Figure 4E and 4F, is there any reason why there is a substantial difference in cellular volume between MDA-MB-231-GFP cells and MDA-MB-231-BR-GFP cells with respect to their characteristics.

Response to Reviewers

We thank the reviewers for their insightful comments to improve our manuscript. Please find each comment listed below and our response. The revised manuscript presents a methodology to glean cellular responses within a microfluidic blood brain niche chip using confocal tomography and machine learning.

Editorial Comments:

Please take this opportunity to thoroughly proofread the manuscript to ensure that there are no spelling or grammatical errors.

Response: The authors have reviewed the manuscript for spelling or grammatical errors.

• ***Protocol Detail:***

1) Please use the imperative voice for ALL steps.

Response: We have amended several sections of the protocol so that it is in the imperative voice for all steps.

2) Please note that your protocol will be used to generate the script for the video, and must contain everything that you would like shown in the video. Please add more specific details (e.g. button clicks for software actions, numerical values for settings, etc) to your protocol steps. There should be enough detail in each step to supplement the actions seen in the video so that viewers can easily replicate the protocol.

Response: We have added more detail to the use of ImageJ to quantify the endothelial barrier coverage of the device in section 4.1. We believe viewers will easily be able to replicate the protocol. We have also expanded sections 7 and 8 to include more specific details of software actions, clicks and settings.

• ***Protocol Numbering:*** **all steps should be lined up at the left margin with no indentations. There must also be a one-line space between each protocol step.**

Response: This has been edited in the manuscript.

• ***Protocol Highlight:*** **After you have made all of the recommended changes to your protocol (listed above), please re-evaluate the length of your protocol section. There is a 10-page limit for the protocol text, and a 3- page limit for filmable content. If your protocol is longer than 3 pages, please highlight ~2.5 pages or less of text (which includes headings and spaces) in yellow, to identify which steps should be visualized to tell the most cohesive story of your protocol steps.**

1) The highlighting must include all relevant details that are required to perform the step. For example, if step 2.5 is highlighted for filming and the details of how to perform the step are given in steps 2.5.1 and 2.5.2, then the sub-steps where the details are provided must be included in the highlighting.

2) The highlighted steps should form a cohesive narrative, that is, there must be a logical flow from one highlighted step to the next.

3) Please highlight complete sentences (not parts of sentences). Include sub-headings and spaces when calculating the final highlighted length.

4) Notes cannot be filmed and should be excluded from highlighting.

Response: Our manuscript Protocol is approximately 8 pages in length. We have highlighted 2.5 pages of the Protocol text for filmable content based on your guidelines. No notes are included in this manuscript and thus are not included in the filmable content.

• ***Discussion:*** **JoVE articles are focused on the methods and the protocol, thus the discussion should be similarly focused. Please ensure that the discussion covers the following in detail and in paragraph form (3-6 paragraphs): 1) modifications and troubleshooting, 2) limitations of the technique, 3) significance with respect to existing methods, 4) future applications and 5) critical steps within the protocol.**

Response: The discussion has been changed to cover each point in detail.

• ***References:*** **Please spell out journal names.**

Response: We have used your endnote library file to format the reference section.

If your figures and tables are original and not published previously or you have already obtained figure permissions, please ignore this comment. If you are re-using figures from a previous publication, you must obtain explicit permission to re-use the figure from the previous publisher (this can be in the form of a letter from an editor or a link to the editorial policies that allows you to re-publish the figure). Please upload the text of the re-print permission (may be copied and pasted from an email/website) as a Word document to the Editorial Manager site in the "Supplemental files (as requested by JoVE)" section. Please also cite the figure appropriately in the figure legend, i.e. "This figure has been modified from [citation]."

Response: We have re-created a figure from a previous article published in Lab on a Chip. Please find included an email from Ms. Chloe Szebrat, a contracts and copyright executive from the Royal Society of Chemistry (RSC) that permits the re-use of figures from this publication. The figure is appropriately cited per RSC guidelines.

Comments from Peer-Reviewers:

Reviewer #1:

<u>Manuscript Summary</u>:

Thanks to authors for sharing their work on this important subject in the form of methods paper.

Response: We thank the reviewer for emphasizing the importance of our research.

<u>Major Concerns:</u>

Authors need to revise their work to have a text that flows in appropriate manner and using correct tense of the verbs. The MS swishes between the use of present and past tense which creates some

confusion. Most of these sections are presented like a recipe which are good for reader and user to follow. However other sections need to be revised, e.g. Sections 3.1., 4.3, 7.2 and 8.3 to mention some examples. Authors need to carefully revise this throughout the MS.

Response: All Protocol sections have been re-written in the imperative voice that included the change of tense of sections 3.1, 4.3, 7.2, 8.3.

Conclusion section should be rewritten to be clear and includes relevant information derived from the study/developed method.

Response: A section of the Conclusion paragraph has been rewritten to initially state the conclusions derived from our study and future work improving the clinical applicability of this platform as a diagnostic towards predicting brain metastases.

Minor Concerns:

Abstract:

"3D models of brain" start sentences with words and not numbers.

Response: The manuscript has been corrected so that all sentences begin with words and not numbers.

Introduction:

"3D structures" write in full, abbreviated words of 3D. Once this is done use abbreviation subsequently, e.g. to replace the full words in "three-dimensional tools" in the second para of the intro sections. Revise all abbreviations and their subsequent use in the MS.

Response: The use of abbreviations has been edited in the manuscript. The term, “Three-dimensional (3D),” has been written out in full in its first use with its abbreviation stated in parentheses, then abbreviated as 3D onwards.

Correct "Independently of migration" to "Independent of migration"

Response: This has been changed in the manuscript.

***Protocol*:**

You may consider changing "made of two sides" to "made of two parts"

Response: The words “sides” or “halves” to describe the upper and lower portions of the device have been changed to “parts” throughout the manuscript.

Correct "Tricholoro perfluoroctyl" to "Trichloro perfluorooctyl"

Response: This has been revised in the manuscript.

Revise the following sentence for clarity "An alternative is to fabricate an aluminum mold the wafer sits inside of to improve flatness and reduce downstream confocal imaging time."

Response: Section 1.9 of the Protocol now states, “Place individual wafer molds into 150 mm petri dishes using two strips of double-sided tape. Ensure the wafers are flat. An alternative is to fabricate an aluminum mold within which the wafer can be placed. Because the aluminum mold is enclosed it will

produce casts with a uniform thickness, whereas the petri dish method is sensitive to the tilt of the surface is it placed on. The improved flatness of the PDMS casts reduces downstream confocal imaging time."

What is the average pore size in the polycarbonate membrane?

Response: The membrane that separates the upper and lower parts of the device has pores of 5 μm average size.

You may consider changing "experimental terminus"

Response: The text has been modified to experimental "timepoint" for clarification.

In section 7.2. instead of citing paper Doi cite as a regular reference

Response: The phrase, "included as a **Supplemental Coding File**" was deleted and a citation to our software package was inserted for reference.

Reviewer #2:

Manuscript Summary:

This is a good manuscript on an implementation to study cellular responses during brain metastasis on blood brain niche using 3D in vitro microfluidic tumor microenvironment model and machine learning technique.

Major Concerns:

Although the authors demonstrated the claim for the novelty of this approach used in the manuscript and showed scientific research in the manuscript, the rationales for the approach are not quite convincing to be published in Journal of Visualized Experiments since there are some experimental designs that need more clarification to rationalize the approach.

Response: We thank the reviewer for their feedback. The rationale to our approach is positioned within the Introduction and aids in the dissemination of this platform and adoption in the field for multiple cellular applications. In particular, we describe 1) the construction of a device to study cancer cells traversing a blood brain barrier into the brain niche, 2) the ability to adapt existing MRI tomography tools to reconstruct 3D representations of the cancer cells within the device, and 3) the utility of machine learning to distinguish between brain-metastatic and non-brain metastatic cancer cell phenotypes based on their response inside the device.

Minor Concerns:

Here are some issues that can help improve this manuscript.

1. It is necessary to more convincingly emphasize why the astrocytic microenvironment should be constructed to recapitulate blood brain niche in terms of physiological relevance.

Response: We appreciate the reviewer's awareness of the contribution of astrocytes in the formation of the blood brain barrier. We added two sentences in the Introduction emphasizing why the astrocytic environment was selected for demonstration of a physiologically relevant blood brain niche: "The blood

brain barrier interface with the brain niche is composed of brain microvascular endothelial cells that are strengthened by basement membrane, astrocyte feet, and pericytes[25]. We selectively focused on the astrocyte and endothelial components given their importance in the formation and regulation of the blood brain barrier. We demonstrate how to fabricate, seed, image, and analyze the cancer cells and tumor micro-environment cellular and humoral components, using this platform."

2. It should be addressed why the measurement of sphericity is important to understand metastatic tumor traits.

Response: A discussion of the traits assessed using confocal tomography is included in the Discussion. "Cancer cell measurements including distance extravasated, percent extravasated by volume, sphericity, and volume are quantified using this technique. Distance extravasated and percent extravasated by volume permit the user to reconstruct the position of the cancer cells within the chip to assess extravasation across the barrier and migration within the tissue. Cell shape measurements such as sphericity and volume are related to the dynamic movements or function of the cell at each timepoint. Migratory MDA-MB-231-BR-GFP cells exhibit a high level of sphericity when initially introduced into the μmBBN device and become less spherical in shape as they decrease their movement and begin to colonize the niche."

3. Figure 3A, there should be more detailed indications for cross-section and top view scheme for this device.

Response: We have introduced two additional schematics for Figure 3A to indicate the top and cross-sectional views of the device.

4. Figure 3B, it is necessary to add an axis title to the horizontal axis in the chart, where high and low mean endothelial coverage of μmBBN devices.

Response: An axis title "Barrier Coverage Classification" was added to Figure 3B.

5. Figure 3C and 3D, there should be an additional scheme for the platform to indicate the location of the endothelial cells layer in the platform.

Response: We have inset schematics of the device into Figures 3C-D to indicate the location of the endothelial cell barrier on the membrane interfacing the top part (flow chamber) and bottom part (brain niche).

6. Figure 3C, it is necessary to demonstrate the representative confocal image, which shows proteins to mark barrier structures such as ZO-1 for a confluent endothelial barrier condition.

Response: We included ZO-1 detection using immunofluorescent imaging of the barrier structure in our initial manuscript published in Lab on a Chip. However, the process of immunofluorescent staining requires fixation of the material for the antibody clones, thus rendering the chip unviable to add cancer cells to. Therefore, we developed the presented method utilizing fluorescence of the endothelial cells represented as cell coverage of the surface area to monitor formation of the endothelial barrier. This alternative technique permits the user to maintain the viability of the endothelial cells and niche layer so that cancer cells are added to the live blood brain niche device once the endothelial cells form a barrier.

7. Figure 4, there should be testing of the statistical significance of results for all graphs.

Response: Significance tests were not reported in the initial manuscript to emphasize its purpose as a methodology, not a hypothesis-driven research article. We found statistical significance between high and low endothelial barrier coverage percentages using a Welch two-sample t-test (Figure 3). We found statistical significance of the μmBBN device dataset for Figure 4 using Pairwise Wilcoxon Rank Sum and Kruskal-Wallis with Dunn's multiple comparisons. Comparisons were made between the brain-seeking MDA-MB-231-BR-GFP and parental MDA-MB-231-GFP cells at each timepoint. The progression of each cancer cell line across timepoints was also included.

8. Figure 4E and 4F, is there any reason why there is a substantial difference in cellular volume between MDA-MB-231-GFP cells and MDA-MB-231-BR-GFP cells with respect to their characteristics.

Response: The appearance of the basal brain-metastatic and parental MDA-MB-231-GFP in 2D culture dishes is different. We believe when cells are challenged in defined conditions, such as our μmBBN device, the plasticity of the brain-metastatic cell line permits cytoskeletal rearrangements to enable extravasation across the BBB that has a direct influence on the cell volume. We have made the following amendment in the Discussion of the manuscript, "Overall cell volume of the MDA-MB-231-GFP and MDA-MB-231-BR-GFP differed due to the difference in shape of the cell lines. Cancer cells that cross the endothelial barrier are more rounded than the cells that do not traverse through the barrier, thus smaller round cells may be able to extravasate across the endothelial layer more efficiently."

Supplemental Figure 1

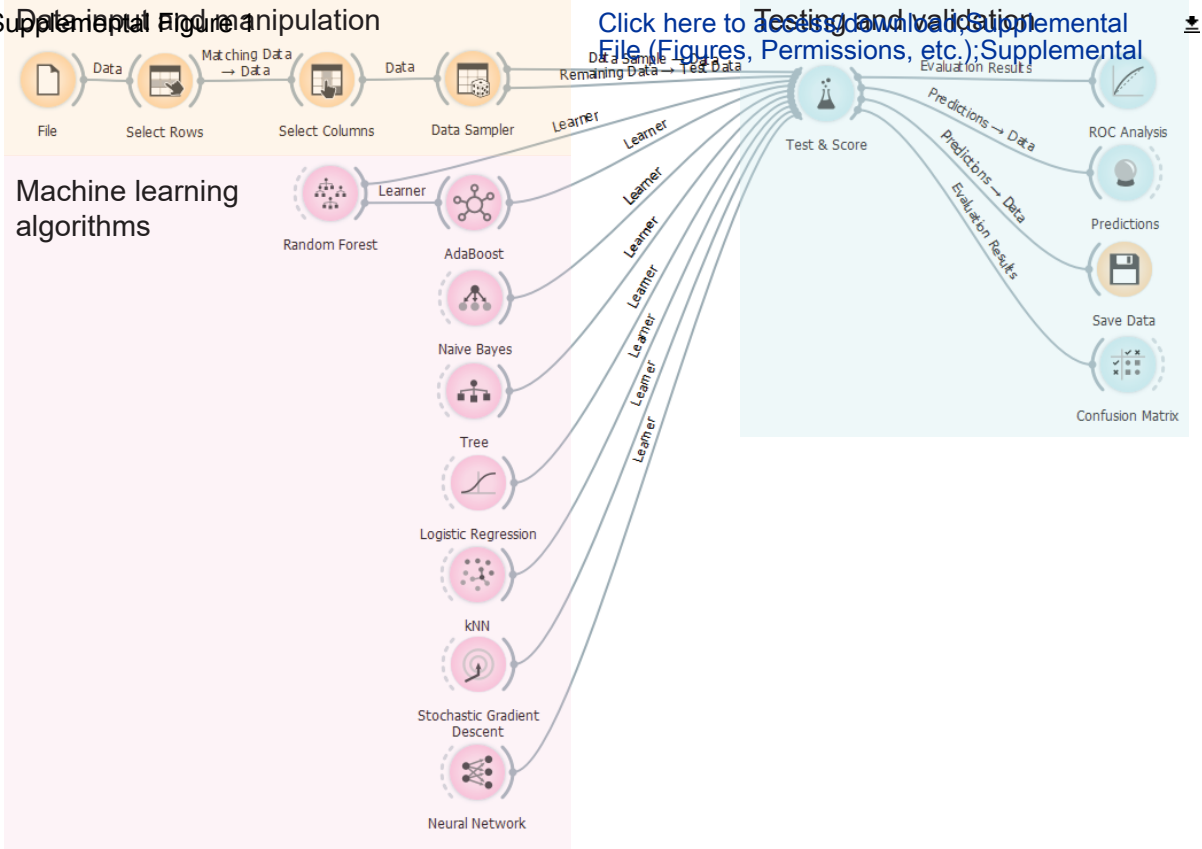

C. Ryan Oliver, PhD is a Research Investigator, at the University of Michigan.

Dr. Oliver received his undergraduate degree from University of Texas Arlington in 2007 and Master degree in 2008 in Industrial and Manufacturing Engineering. He then entered the Mechanical Engineering PhD program, receiving his PhD in 2014 from the University of Michigan.

He then completed his postdoctoral research at Massachusetts Institute of Technology in Dr. John Hart's Mechanosynthesis laboratory. He completed a second postdoctoral training in Dr. Sofia Merajver's lab and Dr. Shuichi Takayama's lab at the University of Michigan. He has since joined the faculty at the University of Michigan in the Internal Medicine Department in the Rogel Cancer Center, where he studies the interplay between Engineering and Cancer Biology to identify translational opportunities.

Trisha Westerhof, PhD is a postdoctoral fellow in the laboratory of Sofia Merajver, MD, PhD, at the University of Michigan, Ann Arbor.

Dr. Westerhof received dual BS degrees in Human Biology and Microbiology & Molecular Genetics from Michigan State University. She completed her PhD in Biological Sciences at the University of California, Irvine under the mentorship of Dr. Edward L. Nelson, MD.

Her research interests are 1) To better understand cancer progression and metastasis at the cellular and molecular levels and 2) To develop novel bio-, nano- and micro-technologies for translation into clinical use.

Maria Castro, PhD is the R.C. Schneider Professor of Neurosurgery, and Professor of Cell and Developmental Biology, at the University of Michigan Medical School.

Dr. Castro received her BSc in Chemistry, dual MSc degrees in Biochemistry and Education Technology, and PhD in Biochemistry at the University of La Plata, Argentina. She completed her postdoctoral training at the National Institute of Child Health and Human Development, NIH, Bethesda, MD, USA.

Her research program focuses on epigenetic regulation of cancer progression, uncovering the role of oncometabolites in the brain tumor microenvironment (TME), and the development of new therapies for adult and pediatric gliomas, including DIPG.

Sofia D. Merajver, PhD, MD is Professor of Internal Medicine and Epidemiology at the University of Michigan, Ann Arbor. She is also the Founder and Director of the Breast and Ovarian Cancer Risk Evaluation Program. Dr. Merajver received her BS degree in Mathematics and then her PhD in Physics (Biophysics) at the University of Maryland. She then received her MD and completed residence in Internal medicine and fellowship in Hematology-Oncology at the University of Michigan. Her research program is focused on integrating molecular genetics of cancer with fundamental studies of the dynamics of cancer signal transduction into innovative clinical strategies for women at high risk for breast cancer and cancer patients. Dr. Merajver has trained over 165 scientists in her laboratory and clinics and is an author in over 300 peer-reviewed manuscripts. Her laboratory has made major discoveries in the molecular genetics of cancer that have impacted our understanding of metastases biology and developmental therapeutics as well as the use of novel computational and physics tools in cancer research.

From: CONTRACTS-COPYRIGHT (shared)
To: tmwester@umich.edu
Subject: RE: copyright permissions question
Date: Wednesday, May 6, 2020 3:58:23 AM

External Email - Use Caution

Many thanks for sending the permissions request below. Under the terms of our licence agreement authors of RSC publications do not have to formally request permission to reproduce figures from their RSC publication in another RSC publication, a non-RSC publication or on a website providing that the correct acknowledgement is included. Please see http://rsc.li/permissions for more details.

Best wishes,

Chloe Szebrat
Contracts and Copyright Executive
Royal Society of Chemistry
Thomas Graham House
Science Park, Milton Road
Cambridge, CB4 0WF, UK
Tel: +44 (0) 1223 438329
www.rsc.org

-----Original Message-----
From: tmwester@umich.edu <tmwester@umich.edu>
Sent: 05 May 2020 14:17
To: CONTRACTS-COPYRIGHT (shared) <Contracts-Copyright@rsc.org>
Subject: copyright permissions question

Name: Trisha Westerhof
Message: Hi RSC, my colleagues and I were invited to submit a video protocol manuscript to JoVE based on our work published in a Lab on a Chip paper, https://pubs.rsc.org/en/content/articlelanding/2019/LC/C8LC01387J#!divAbstract
We have re-created a figure that was included in our LoC paper for use in the JoVE paper. I would like confirmation if we do or do not need to request permission from RSC to re-publish this data, and if we do need to make a request, where is the form I need to complete?

Thank you

PDMS mold drawing

Alignment fixture drawing

Click here to access/download
Supplemental Coding Files
Supplemental File 2.DXF

1 Alewife Center #200
Cambridge, MA 02140
tel. 617.945.9051
www.jove.com

ARTICLE AND VIDEO LICENSE AGREEMENT

Title of Article:	Quantifying the brain metastatic tumor micro-environment using an organ-on-a chip 3D model, machine learning, and confocal tomography.
Author(s):	C. Ryan Oliver, Trisha M. Westerhof, Maria G. Castro, Sofia D. Merajver

Item 1: The Author elects to have the Materials be made available (as described at http://www.jove.com/publish) via:

☑ Standard Access ☐ Open Access

Item 2: Please select one of the following items:

☒ The Author is **NOT** a United States government employee.

☐ The Author is a United States government employee and the Materials were prepared in the course of his or her duties as a United States government employee.

ARTICLE AND VIDEO LICENSE AGREEMENT

1. **Defined Terms.** As used in this Article and Video License Agreement, the following terms shall have the following meanings: "**Agreement**" means this Article and Video License Agreement; "**Article**" means the article specified on the last page of this Agreement, including any associated materials such as texts, figures, tables, artwork, abstracts, or summaries contained therein; "**Author**" means the author who is a signatory to this Agreement; "**Collective Work**" means a work, such as a periodical issue, anthology or encyclopedia, in which the Materials in their entirety in unmodified form, along with a number of other contributions, constituting separate and independent works in themselves, are assembled into a collective whole; "**CRC License**" means the Creative Commons Attribution-Non Commercial-No Derivs 3.0 Unported Agreement, the terms and conditions of which can be found at: http://creativecommons.org/licenses/by-nc-nd/3.0/legalcode; "**Derivative Work**" means a work based upon the Materials or upon the Materials and other pre-existing works, such as a translation, musical arrangement, dramatization, fictionalization, motion picture version, sound recording, art reproduction, abridgment, condensation, or any other form in which the Materials may be recast, transformed, or adapted; "**Institution**" means the institution, listed on the last page of this Agreement, by which the Author was employed at the time of the creation of the Materials; "**JoVE**" means MyJove Corporation, a Massachusetts corporation and the publisher of The Journal of Visualized Experiments; "**Materials**" means the Article and / or the Video; "**Parties**" means the Author and JoVE; "**Video**" means any video(s) made by the Author, alone or in conjunction with any other parties, or by JoVE or its affiliates or agents, individually or in collaboration with the Author or any other parties, incorporating all or any portion of the Article, and in which the Author may or may not appear.

2. **Background.** The Author, who is the author of the Article, in order to ensure the dissemination and protection of the Article, desires to have the JoVE publish the Article and create and transmit videos based on the Article. In furtherance of such goals, the Parties desire to memorialize in this Agreement the respective rights of each Party in and to the Article and the Video.

3. **Grant of Rights in Article.** In consideration of JoVE agreeing to publish the Article, the Author hereby grants to JoVE, subject to **Sections 4** and **7** below, the exclusive, royalty-free, perpetual (for the full term of copyright in the Article, including any extensions thereto) license (a) to publish, reproduce, distribute, display and store the Article in all forms, formats and media whether now known or hereafter developed (including without limitation in print, digital and electronic form) throughout the world, (b) to translate the Article into other languages, create adaptations, summaries or extracts of the Article or other Derivative Works (including, without limitation, the Video) or Collective Works based on all or any portion of the Article and exercise all of the rights set forth in (a) above in such translations, adaptations, summaries, extracts, Derivative Works or Collective Works and(c) to license others to do any or all of the above. The foregoing rights may be exercised in all media and formats, whether now known or hereafter devised, and include the right to make such modifications as are technically necessary to exercise the rights in other media and formats. If the "Open Access" box has been checked in **Item 1** above, JoVE and the Author hereby grant to the public all such rights in the Article as provided in, but subject to all limitations and requirements set forth in, the CRC License.

4. **Retention of Rights in Article.** Notwithstanding the exclusive license granted to JoVE in **Section 3** above, the Author shall, with respect to the Article, retain the non-exclusive right to use all or part of the Article for the non-commercial purpose of giving lectures, presentations or teaching classes, and to post a copy of the Article on the Institution's website or the Author's personal website, in each case provided that a link to the Article on the JoVE website is provided and notice of JoVE's copyright in the Article is included. All non-copyright intellectual property rights in and to the Article, such as patent rights, shall remain with the Author.

5. **Grant of Rights in Video – Standard Access.** This **Section 5** applies if the "Standard Access" box has been checked in **Item 1** above or if no box has been checked in **Item 1** above. In consideration of JoVE agreeing to produce, display or otherwise assist with the Video, the Author hereby acknowledges and agrees that, Subject to **Section 7** below, JoVE is and shall be the sole and exclusive owner of all rights of any nature, including, without limitation, all copyrights, in and to the Video. To the extent that, by law, the Author is deemed, now or at any time in the future, to have any rights of any nature in or to the Video, the Author hereby disclaims all such rights and transfers all such rights to JoVE.

6. **Grant of Rights in Video – Open Access.** This **Section 6** applies only if the "Open Access" box has been checked in **Item 1** above. In consideration of JoVE agreeing to produce, display or otherwise assist with the Video, the Author hereby grants to JoVE, subject to **Section 7** below, the exclusive, royalty-free, perpetual (for the full term of copyright in the Article, including any extensions thereto) license (a) to publish, reproduce, distribute, display and store the Video in all forms, formats and media whether now known or hereafter developed (including without limitation in print, digital and electronic form) throughout the world, (b) to translate the Video into other languages, create adaptations, summaries or extracts of the Video or other Derivative Works or Collective Works based on all or any portion of the Video and exercise all of the rights set forth in (a) above in such translations, adaptations, summaries, extracts, Derivative Works or Collective Works and (c) to license others to do any or all of the above. The foregoing rights may be exercised in all media and formats, whether now known or hereafter devised, and include the right to make such modifications as are technically necessary to exercise the rights in other media and formats. For any Video to which this **Section 6** is applicable, JoVE and the Author hereby grant to the public all such rights in the Video as provided in, but subject to all limitations and requirements set forth in, the CRC License.

7. **Government Employees.** If the Author is a United States government employee and the Article was prepared in the course of his or her duties as a United States government employee, as indicated in **Item 2** above, and any of the licenses or grants granted by the Author hereunder exceed the scope of the 17 U.S.C. 403, then the rights granted hereunder shall be limited to the maximum rights permitted under such statute. In such case, all provisions contained herein that are not in conflict with such statute shall remain in full force and effect, and all provisions contained herein that do so conflict shall be deemed to be amended so as to provide to JoVE the maximum rights permissible within such statute.

8. **Protection of the Work.** The Author(s) authorize JoVE to take steps in the Author(s) name and on their behalf if JoVE believes some third party could be infringing or might infringe the copyright of either the Author's Article and/or Video.

9. **Likeness, Privacy, Personality.** The Author hereby grants JoVE the right to use the Author's name, voice, likeness, picture, photograph, image, biography and performance in any way, commercial or otherwise, in connection with the Materials and the sale, promotion and distribution thereof. The Author hereby waives any and all rights he or she may have, relating to his or her appearance in the Video or otherwise relating to the Materials, under all applicable privacy, likeness, personality or similar laws.

10. **Author Warranties.** The Author represents and warrants that the Article is original, that it has not been published, that the copyright interest is owned by the Author (or, if more than one author is listed at the beginning of this Agreement, by such authors collectively) and has not been assigned, licensed, or otherwise transferred to any other party. The Author represents and warrants that the author(s) listed at the top of this Agreement are the only authors of the Materials. If more than one author is listed at the top of this Agreement and if any such author has not entered into a separate Article and Video License Agreement with JoVE relating to the Materials, the Author represents and warrants that the Author has been authorized by each of the other such authors to execute this Agreement on his or her behalf and to bind him or her with respect to the terms of this Agreement as if each of them had been a party hereto as an Author. The Author warrants that the use, reproduction, distribution, public or private performance or display, and/or modification of all or any portion of the Materials does not and will not violate, infringe and/or misappropriate the patent, trademark, intellectual property or other rights of any third party. The Author represents and warrants that it has and will continue to comply with all government, institutional and other regulations, including, without limitation all institutional, laboratory, hospital, ethical, human and animal treatment, privacy, and all other rules, regulations, laws, procedures or guidelines, applicable to the Materials, and that all research involving human and animal subjects has been approved by the Author's relevant institutional review board.

11. **JoVE Discretion.** If the Author requests the assistance of JoVE in producing the Video in the Author's facility, the Author shall ensure that the presence of JoVE employees, agents or independent contractors is in accordance with the relevant regulations of the Author's institution. If more than one author is listed at the beginning of this Agreement, JoVE may, in its sole

discretion, elect not take any action with respect to the Article until such time as it has received complete, executed Article and Video License Agreements from each such author. JoVE reserves the right, in its absolute and sole discretion and without giving any reason therefore, to accept or decline any work submitted to JoVE. JoVE and its employees, agents and independent contractors shall have full, unfettered access to the facilities of the Author or of the Author's institution as necessary to make the Video, whether actually published or not. JoVE has sole discretion as to the method of making and publishing the Materials, including, without limitation, to all decisions regarding editing, lighting, filming, timing of publication, if any, length, quality, content and the like.

12. **Indemnification.** The Author agrees to indemnify JoVE and/or its successors and assigns from and against any and all claims, costs, and expenses, including attorney's fees, arising out of any breach of any warranty or other representations contained herein. The Author further agrees to indemnify and hold harmless JoVE from and against any and all claims, costs, and expenses, including attorney's fees, resulting from the breach by the Author of any representation or warranty contained herein or from allegations or instances of violation of intellectual property rights, damage to the Author's or the Author's institution's facilities, fraud, libel, defamation, research, equipment, experiments, property damage, personal injury, violations of institutional, laboratory, hospital, ethical, human and animal treatment, privacy or other rules, regulations, laws, procedures or guidelines, liabilities and other losses or damages related in any way to the submission of work to JoVE, making of videos by JoVE, or publication in JoVE or elsewhere by JoVE. The Author shall be responsible for, and shall hold JoVE harmless from, damages caused by lack of sterilization, lack of cleanliness or by contamination due to the making of a video by JoVE its employees, agents or independent contractors. All sterilization, cleanliness or decontamination procedures shall be solely the responsibility of the Author and shall be undertaken at the Author's expense. All indemnifications provided herein shall include JoVE's attorney's fees and costs related to said losses or damages. Such indemnification and holding harmless shall include such losses or damages incurred by, or in connection with, acts or omissions of JoVE, its employees, agents or independent contractors.

13. **Fees.** To cover the cost incurred for publication, JoVE must receive payment before production and publication of the Materials. Payment is due in 21 days of invoice. Should the Materials not be published due to an editorial or production decision, these funds will be returned to the Author. Withdrawal by the Author of any submitted Materials after final peer review approval will result in a US$1,200 fee to cover pre-production expenses incurred by JoVE. If payment is not received by the completion of filming, production and publication of the Materials will be suspended until payment is received.

14. **Transfer, Governing Law.** This Agreement may be assigned by JoVE and shall inure to the benefits of any of JoVE's successors and assignees. This Agreement shall be governed and construed by the internal laws of the Commonwealth of Massachusetts without giving effect to any conflict of law provision thereunder. This Agreement may be executed in counterparts, each of which shall be deemed an original, but all of which together shall be deemed to me one and the same agreement. A signed copy of this Agreement delivered by facsimile, e-mail or other means of electronic transmission shall be deemed to have the same legal effect as delivery of an original signed copy of this Agreement.